2010

Automatic multi-resolution spatio-frequency mottle metric (sfmm) for evaluation of macrouniformity

Siddharth Khullar

AUTOMATIC MULTI-RESOLUTION SPATIO-FREQUENCY MOTTLE METRIC (SFMM) FOR EVALUATION OF MACROUNIFORMITY

by

Siddharth Khullar

A Graduate Thesis Submitted in Partial Fulfillment of the

Requirements for the Degree of

MASTER OF SCIENCE

In

ELECTRICAL ENGINEERING

Approved by:

Prof. _____

Thesis Advisor – Dr. Eli Saber

Prof. _____

Thesis Committee Member – Dr. Sohail A. Dianat

Prof. _____

Thesis Committee Member – Dr. Stefi Baum (Center for Imaging Science)

Prof. _____

Department Head – Dr. Sohail A. Dianat

Department of Electrical & Microelectronics Engineering,

The Kate Gleason College of Engineering,

Rochester Institute of Technology,

Rochester, New York

March, 2010

THESIS AUTHOR PERMISSION STATEMENT

Title of Thesis : Automatic Multi-Resolution Spatio-Frequency Mottle Metric (SFMM) for Evaluation of Macrouniformity.
Name of Author : Siddharth Khullar
Degree : Master of Science
Program : Electrical Engineering
College : Kate Gleason College of Engineering

I understand that I must submit a print copy of my thesis or dissertation to the RIT Archives, per current RIT guidelines for the completion of my degree. I hereby grant to the Rochester Institute of Technology and its agents the non-exclusive license to archive and make accessible my thesis or dissertation in whole or in part in all forms of media in perpetuity. I retain all other ownership rights to the copyright of the thesis or dissertation. I also retain the right to use in future works (such as articles or books) all or part of this thesis or dissertation.

Print Reproduction Permission Granted:
I, **Siddharth Khullar**, hereby **grant permission** to the Rochester Institute Technology to reproduce my print thesis or dissertation in whole or in part. Any reproduction will not be for commercial use or profit.

Signature of Author: _____ Date: _____

Inclusion in the RIT Digital Media Library Electronic Thesis & Dissertation (ETD) Archive
I, **Siddharth Khullar**, additionally grant to the Rochester Institute of Technology Digital Media Library (RIT DML) the non-exclusive license to archive and provide electronic access to my thesis or dissertation in whole or in part in all forms of media in perpetuity.
I understand that my work, in addition to its bibliographic record and abstract, will be available to the world-wide community of scholars and researchers through the RIT DML. I retain all other ownership rights to the copyright of the thesis or dissertation. I also retain the right to use in future works (such as articles or books) all or part of this thesis or dissertation. I am aware that the Rochester Institute of Technology does not require registration of copyright for ETDs.
I hereby certify that, if appropriate, I have obtained and attached written permission statements from the owners of each third party copyrighted matter to be included in my thesis or dissertation. I certify that the version I submitted is the same as that approved by my committee.

Signature of Author: _____ Date: _____

DEDICATION

This thesis is dedicated to my parents

To my father, Mr. Rajesh Khullar, for his unparalleled and unique ways of motivating me from time to time

To my mother, Mrs. Rina Khullar, for her never ending love

And to my best friend

Ms. Shilpa Tyagi for always being there for me

ACKNOWLEDGMENTS

I feel it to be a unique privilege combined with immense happiness to acknowledge the contributions and support of all the wonderful people who have been responsible for the completion of my master's degree. The two years of graduate study at RIT has taught me that creative instinct, excellent fellowship and perceptiveness are the very essence of engineering. It not only imparts knowledge but also lays emphasis on the overall development of an individual. I am extremely appreciative of RIT, especially Department of Electrical Engineering in this regard.

I would like to thank Dr. Sohail Dianat, Dr. Eric Peskin and Dr. Stefi Baum for their valuable assistance that has made this work possible. Also, I extend my sincerest gratitude to all my friends/colleagues in and outside the 'signal processing community' at RIT for their encouragement and being a part of a grueling yet enjoyable educational experience. I am grateful to Mr. Robert Lawton and Mr. Jeff Trask and the Hewlett Packard Company for their generosity in supporting and sponsoring this research and showing tremendous confidence and satisfaction in my work and the results achieved.

Finally, I am extremely indebted to the man whose unique ways of teaching and relentless guidance is solely responsible for transmuting an ordinary student like me to a confident graduate researcher. His inspired notion that "if intellect can find the right question, learning and research help find the answer, seek and thou shall find", has been instrumental in what I am today. Thank you Dr. Eli Saber for everything that you have done for me, it's been a pleasure being your student.

Siddharth Khullar

ABSTRACT

Evaluation of mottle is an area of on-going research in print quality assessment. We propose an unsupervised evaluation technique and a metric that measures mottle in a hard-copy laser print. The proposed algorithm uses a scanned image to quantify the low frequency variation or mottle in what is supposed to be a uniform field. 'Banding' and 'Streaking' effects are explicitly ignored and the proposed algorithm scales the test targets from "Flat print" (Good) to "Noisy print" (Bad) based on mottle only. The evaluation procedure is modeled as feature computation in different combinations of spatial, frequency and wavelet domains.

The model is primarily independent of the nature of the input test target, i.e. whether it is chromatic or achromatic. The algorithm adapts accordingly and provides a mottle metric for any test target. The evaluation process is done using three major modules: (1) Pre-processing Stage, which includes acquisition of the test target and preparing it for processing; (2) Spatio-frequency Parameter Estimation where different features characterizing mottle are calculated in spatial and frequency domains; (3) Invalid Feature Removal Stage, where the invalid or insignificant features (in context to mottle) are eliminated and the dataset is ranked relatively.

The algorithm was demonstrated successfully on a collection of 60 K-Only printed images spread over 2 datasets printed on 3 different faulty printers and 4 different media Also, it was tested on 5 color targets for the color version of the algorithm printed using 2 different printers and 5 different media, provided by Hewlett Packard Company.

TABLE OF CONTENTS

LIST OF FIGURES

LIST OF TABLES

Chapter 1: Introduction

Print mottle is a common defect occurring in the printing industry. It is mostly associated with printing on paper, but can be observed on all printed surfaces, whether porous, like paper, or solid. This thesis addresses a class of defects known as mottle. Perceptually, mottle is defined as perceived non-homogeneities in the print due to unintentional variations in the lightness of the printed surface when it is viewed under homogenous illumination. Objectively, mottle is a laterally varying reflectance in homogenous tone areas that expresses itself as stochastic blobs or cloudiness or sometimes graininess-type patterns.

The characterization and evaluation of print mottle is a crucial step in the assessment of the printing quality of papers and boards. This assessment is however a subjective phenomenon and is usually evaluated by a set of independent observers. For practical purposes, it is nevertheless desirable to have a reliable way of establishing a mottle index through mathematical image analysis of the digitized printed samples. This allows the paper maker to compare different types of furnish, coating layer, operating conditions etc., and to analyze their relative importance in the formation of print mottles. It is then of course imperative that the mathematical discretization and evaluation of mottle correlates well with the visual ranking of the same samples by a group of observers.

1.1. Motivation

Measurement of print quality is essential in many applications such as development of print-defect detection algorithms and photographic printing. It is imperative for print

engines in use today to meet stable image quality requirements as evaluated by various metrics. The current marketplace demands the best image quality at competitive costs with minimum downtime. Hence, the ability for print engine vendors to efficiently achieve the highest levels of quality will ensure them a leadership role in the printing industry.

Ordinarily, these measurements are made by a Print Quality Expert (PQE) using various psychometric techniques and methods. Unsupervised measurement of print quality is a topic widely being worked upon by most scientists in this field and has yielded impressive results. The characterization and evaluation of print mottle is an important step in assessment of print quality and is also the parameter of a hard copy print. Even though print engines are thoroughly tested during the manufacturing process, occurrence of mottle remains inevitable usually due to the uneven ink lay or non-uniform ink absorption across the paper surface, especially visible in mid-tone imagery or areas of uniform color such as solids and continuous-tone screen builds.

Many evaluation models have been proposed for assessment of print quality in the past. Initial approaches include band-pass analysis, texture analysis, and measurement of specific perimeter and coefficient of variation. Some of the most common structural artifacts are banding, streaking, mottle, Debris-Centered Deletion (DCD) and debris missing DCD's as seen in electro-photographic (EP) engines [1]. ISO-13660 [2] is the first international standard to incorporate a wide range of print quality attributes. ISO 13660 and ISO 19751 [3, 4] define standards and measurement procedures for some basic print quality attributes and artifacts such as streaks, banding, mottle, color rendition, text and line quality, and gloss. Applications and limitations of the ISO-13660 are discussed

in [5, 6, 7, and 8]. Every printing technology has different print quality characteristics [9] and different print artifacts.

Johansson [10] proposed a method based upon the spatial wavelength analysis and named it as Band Pass Analysis (BPA). A modified coefficient of variation highlighting the effect of mean reflectance on print mottle was proposed by Fahlcrantz et al. [11]. The authors claim the method proposed in [10] overestimates the mottle in dark prints but underestimates the lighter ones. Based on theoretical evidence and empirical testing, authors in [11] propose a square-root dependency of perceived luminance level on physical luminance level instead of the original cube-root relation in the CIELAB equation [11]. Moving to evaluation of systematic print mottle, Fahlcrantz [12] proposed a model to evaluate variations that were systematic in nature. The model considered the variation between wavelengths of 0.25 and 16 mm and used a Contrast Sensitivity Function (CSF) of the HVS (Human Visual System) in form of a weighting vector to adjust variation in sensitivities at different frequencies. This model lacked the ability to perform a local analysis of printed area, and was also sensitive to half-tone screening defects due to its sensitivity to high frequencies.

All the above methods are also compared by Fahlcrantz et al. [13]. They conceptually examine and compare different techniques including ISO/IEC 13660 to postulate all aspects governing visual print-quality assessment and also question the need of a model-dependent ISO standard with emphasis laid upon whether ISO 13660 is a complete standard or not. ISO 13660 being based on density variations divides the evaluation model into two measurements – Graininess and Mottle, based on crude-band pass partitioning where higher frequencies correspond to the former and lower

frequencies correspond to the latter, the partition threshold is set at 0.4 cycles/mm (~10 cycles/inch).

More recently proposed color mottle evaluation metric [14, 15] is based on prior work done in the grayscale domain. However, the evaluation of color mottle is done by assuming conditional independence of channel information. In this thesis, we evaluate mottle in test targets printed using K component only in CMYK printers.

Techniques based on multi-scale and multi-resolution analysis have long been in existence in reference to print quality. Eid et al. [16] utilized a combination of the Discrete Wavelet Transform (DWT) and the ISO/IEC 13660. The results of this technique prove to be a lot better than those of ISO/IEC 13660. Another approach proposed by Donohue et al. [17] examines the wavelet analysis exploiting its localized spatio-frequency properties for characterizing defects of limited spatial support.

Current printing environments utilize trained PQEs to visually inspect a subset of the output documents in order to ensure that customer hardcopies are free of defects such as mottle, banding and streaks that tend to hinder the efficient flow of business in print shops for instance. PQE are trained to spot these defects and render an initial classification. This process is generally prone to errors, high costs, time consuming, inherently variable and often subjective [18]. To minimize these problems, an automated mottle analysis system is essential for Quality Assurance (QA). Such a system will help the PQE to quickly and objectively locate and quantify mottle with the aid of a scanner and thereby select the proper diagnostic procedure in an automated fashion to render a corrective action as swiftly as possible. In addition, the system should be user friendly and designed for commercial use producing accurate results. Such an automated QA

system would prove invaluable for testing, calibrating, benchmarking, monitoring applications and optimizing service intervals.

A number of automated mottle quantification systems have been proposed and are categorized into either reference QA systems, where a printed output is compared to a reference image to analyze image quality, or blind QA systems, where the quality of an image is analyzed without a reference image [19]. In [20], a device independent reference QA system was developed to analyze the print quality produced by any printing technology. Many device dependent reference QA systems [21-23] are designed for a specific printer or a specific ink type in the past. Most of them were laboratory systems used only in development and research studies or requires special hardware. Also, Streckel *et al* [24] proposed an objective print quality assessment system to measure density variations and print artifacts like mottle, granularity, streaks, banding, and satellites. A flatbed scanner is used to capture hardcopies of a flat test target. This system is only limited to test patterns and used for comparing print fidelity between different printing machines and technologies.

1.2. Contributions

The main goal throughout the work has been to present a general objective model that can measure print mottle in a way that corresponds well with the way in which it is perceived by human observers. A solid print is usually composed of several zones of lighter or darker areas around a certain mean where the size and the orientation of these zones are random.

An outline of the proposed algorithm primarily consisting of 3 modules is shown in Fig. 1. The first module (M1) is known as the pre-processing module and is responsible

for preparing the input image for feature calculation. We make use of a multi-resolution approach (dyadic wavelets based) to generate a de-noised perceptual approximation from the input image and further process this image in the spatial and frequency domain separately, resulting in several features characterizing mottle. In the case of colored test targets, we insert a Principal Component Analysis (PCA) phase to primarily find the principal component and provide it as the input image to the next module. The second module, spatio-frequency parameter estimation (M2) handles feature computation in both, spatial and frequency domains and provides the third module (M3) with an a priori dataset to sort and remove invalid features. An effective Invalid Feature Removal (IFR) technique facilitates the algorithm to result in a meaningful mottle number by removing the features which do not characterize the non-uniformity of test targets. Algorithm's performance evaluation is done by comparing ranks of the final metric against each target's visual scaling results, and a measure of performance is calculated in terms of correlation between the measured value and the visual scaling.

In this thesis, a novel methodology is proposed, to quantify mottle for K-only hard-copy prints and, associate a mottle number with each test target, known as the Spatio-Frequency Mottle Metric or SFMM. The metric is divided in to two categories: (1) Relative SFMM - for several test targets evaluated and rank ordered with respect to each other; (2) Absolute SFMM – for a single test target randomly picked from a data set and evaluated independently. In our previous work [37], a method to only evaluate mottle on a relative scale using six spatial and frequency spectrum based features (ring mottle, spectral entropy, angular second moment, inverse difference moment, spatial entropy and SFDA feature proposed by Rosenberger [see 34]) was described. The method in [37] was

only validated on a set of 10 test targets. For the proposed algorithm, a new set of eleven features (including the aforementioned six features) is computed using gray level run-length matrices (short run emphasis, long run emphasis, gray level non-uniformity, run length non-uniformity, and run percentage), explained in detail in Chapter 2. These features are further utilized to compute two different mottle numbers– 'Relative SFMM' and 'Absolute SFMM'. The algorithm was tested on two different data sets – (1) a small data set of 10 targets and (2) a larger dataset of 50 test targets, produced from combinations of 3 different printers and 4 types of media. The algorithm is initiated in a pre-processing step (cropping and de-noising) followed by computation of the features mentioned above. Second, an insignificant feature removal module removes feature(s) which are non-significant of mottle across that particular set of test targets (data set 1 or 2). The final set of features are added together to yield a single number (known as the SFMM) followed by rank ordering of these SFMM values on a relative scale by utilizing the ranking module in the algorithm. The above steps are explained in detail in Chapter 2. Another drawback seen in literature was the absence of an absolute objective mottle metric, that characterizes a single target alone and not on a relative scale of several test targets. For this purpose, a novel log-weighted absolute metric (Absolute SFMM) is proposed here (see Figure 1), also explained in Chapter 2.

The importance of the current need for a stable and robust print quality model was presented hereby summarizing some of the benchmark work done in the past several years. Although, these techniques have shown significant improvements over their predecessors, there is still not a single standard in this field that is being used universally.

The proposed SFMM algorithm is designed for flat prints and not halftones giving a better representation of how much mottle was introduced by each printer on each media.

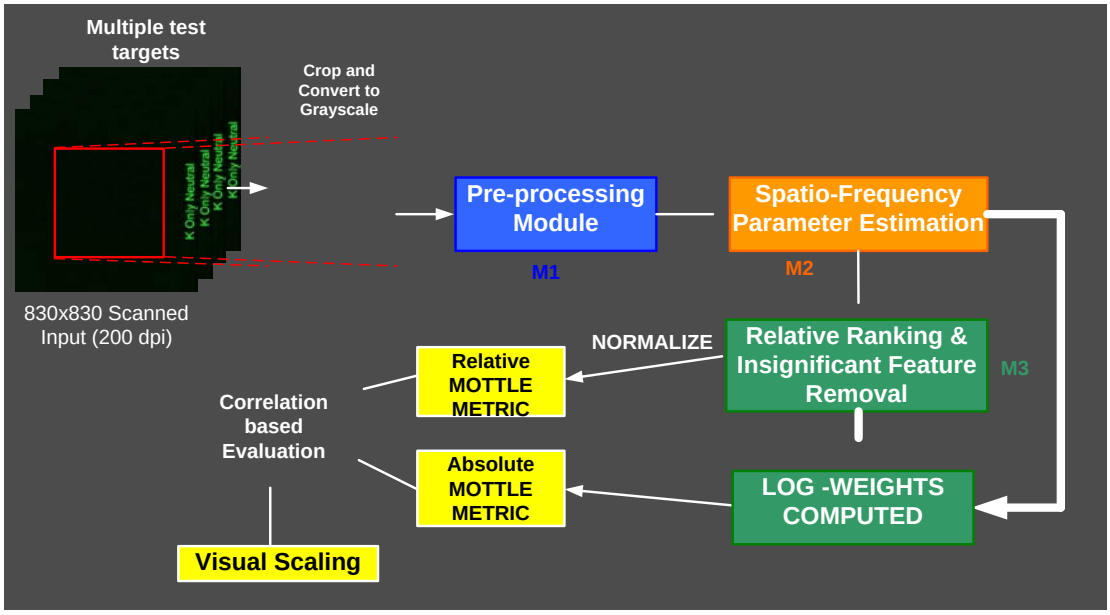

Figure 1: Overview of the proposed algorithm, showing all modules and output of the algorithm.

The detection of mottle is almost impossible in text areas and 'busy' real life images but it is clearly visible in 'flatter' areas of the image like skies or homogeneous background. Therefore, the proposed algorithm is validated on targets that are primarily flat or contain large homogeneous regions.

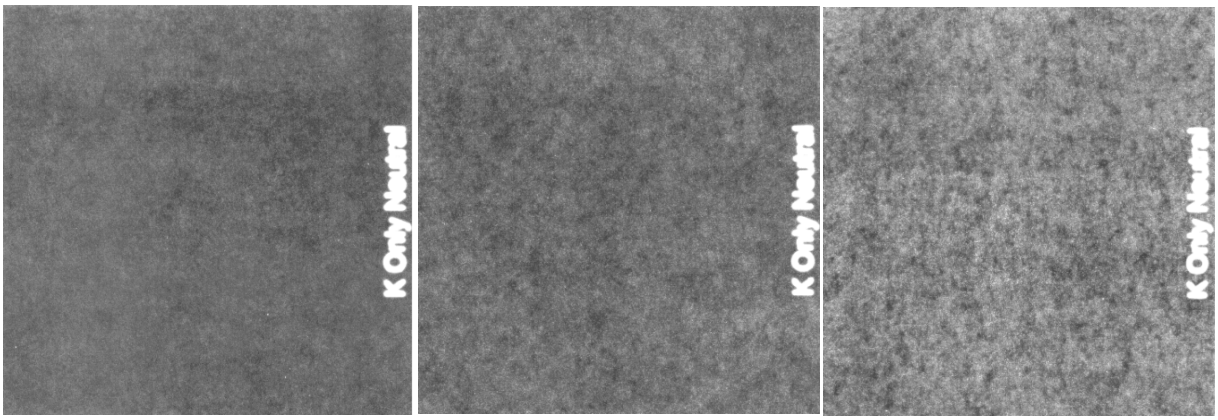

Figure 2: Overview of the test targets and the varying scale of mottle in them.

A few of the test targets after contrast enhancement are shown in Figure 2. Notice, that they are arranged in order of increasing amount of mottle.

Further, in this thesis we propose an extension of the above work to evaluate color mottle by utilizing a computationally simplistic PCA-based approach. As there is a need for subjective evaluations of color test targets before reporting the method's accuracy, we present five color test targets in a contrast enhanced manner along with their respective PCs for the reader to compare the objective evaluation with their own visual ranking.

We present a case study to evaluate mottle in color samples printed using CMYK printing systems. The idea behind this analysis is implemented by inclusion of a PCA based module added to the existing SFMM algorithm. The samples used for the color mottle analysis is shown in Figure 3 below.

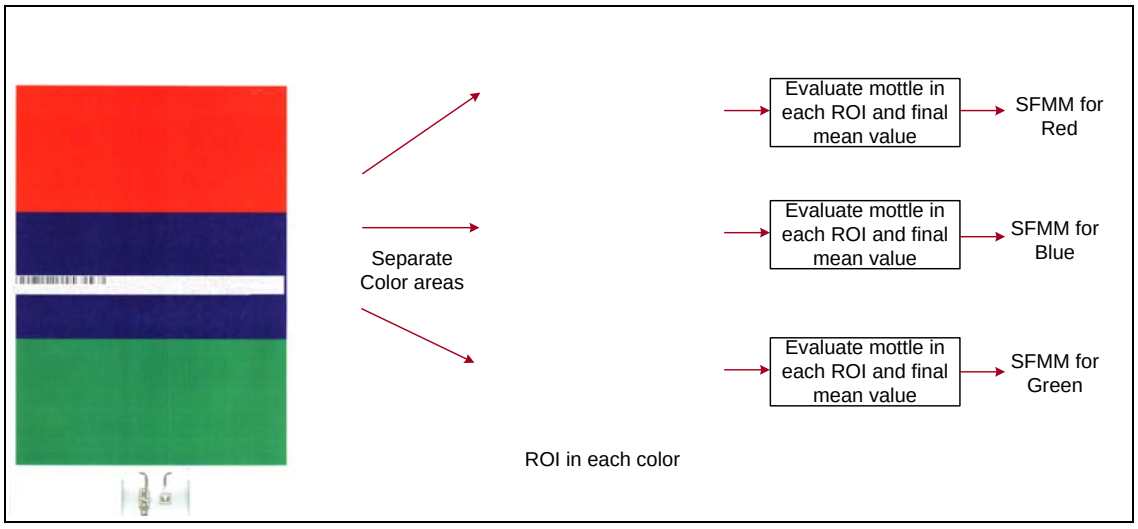

Figure 3: Evaluation methodology for the given design pattern of color print samples. There are in total 5 samples such as these on similar type of media.

1.3. Thesis Organization

The remainder of this thesis is organized as follows: Chapter 2 describes the acquisition and pre-processing of input images obtained from hard copy prints, outlines

the spatio-frequency parameter estimation process and introduces the insignificant feature removal process. Chapter 3 presents the new method for evaluation of mottle in color hard copy prints. All results are presented and discussed in Chapter 4. Finally, conclusions are drawn in Chapter 5.

Chapter 2: Theoretical Development

This chapter is presented in 6 subsections: Image Acquisition, Image Pre-processing, Spatio-frequency Parameter Estimation, Ranking Algorithm, Insignificant Feature Removal and conclusively the computation procedures of 'Relative SFMM and 'Absolute SFMM'. It is imperative to know that the theories explained in this chapter have laid the foundation for this work and are the fundamental steps to compute the mottle metric known as the SFMM.

2.1. Image Acquisition

Since, the objective of this work is to develop a device independent QA system, all the input images need to be calibrated post-acquisition due to the artifacts introduced due to the image capture system, in this, a scanner. This calibration can be done in two ways: (1) matrix transformations using color CIELAB color space or (2) by using scanners that perform the calibration right after the lamps acquire the image and right before it is converted into a software-readable format like TIFF or BMP.

Each test page consists of two targets - (1) K (black) only and (2) Process Neutral, scanned at 200 dpi. The scanner used is HP Scanjet G4010 controlled by a 'back-door' code to set parameters of the scanner. Each test target is acquired twice, once with all 6 lamps active and subsequently with two green lamps active. Note that, the green lamp is the most sensitive to non-uniformities in luminance values. This advantage of the scanner eliminates the need for calibration. Two separate TIFF files (*printer_media_K.tif &*

printer_media_N.tif) are generated from each test page. The block diagram in Figure 4 explains the above process.

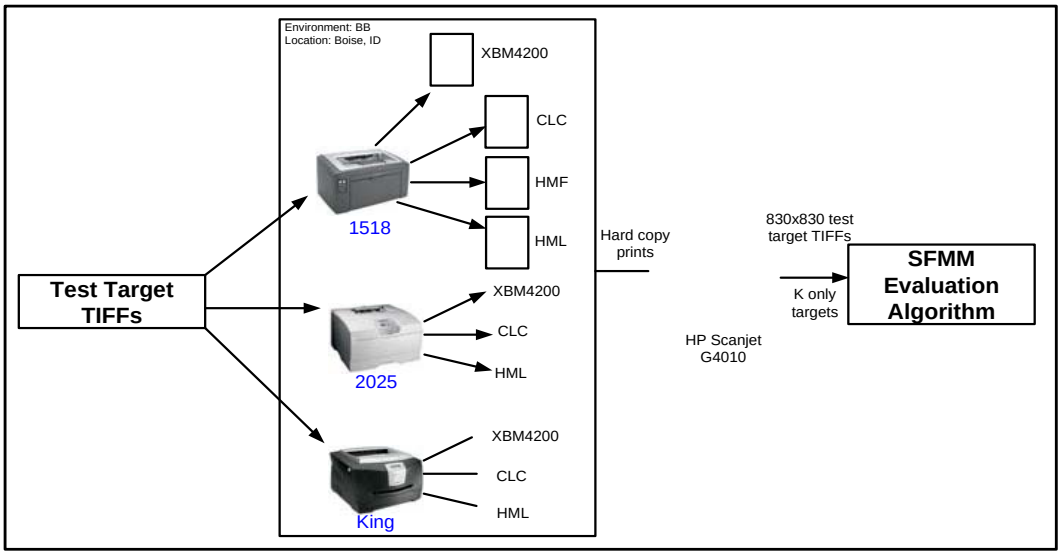

Figure 4: Steps involved in producing test hard-copies and their acquisition for mottle evaluation.

2.2. Image Pre-processing

The results of this work highly depended on how true the input images were. The comparison criterion is subjective rankings (PQEs) of these test targets against the SFMM rankings. Hence, it becomes important to make sure that the input image is utilized to compute texture features such that these features correspond to the observations made by PQEs, therefore, making the model reliable and useful universally.

The input image acquired from the scanner has dimensions about 830x830 and is saved as a TIFF file. This image is converted to grayscale using the MATLAB® routine:

$$I_{gray} = 0.2989R + 0.5870G + 0.1140B \quad (1)$$

where I_{gray} is the final grayscale image and [R, G, B] are three channels of the TIFF file input from scanner. Note that the coefficient of the green channel is greater than the other

two coefficients because the green channel is more highly sensitive to changes in luminance values than the other two channels. The red and blue channels are included in the input image as they may contain variation information which could be lost on selecting only the green channel. The resultant grayscale image is cropped with respect to center of the original image as shown in Figure 5 such that the features can be computed efficiently. Next, the image obtained here goes through the wavelet de-noising stage which comprises the most significant portion of this module.

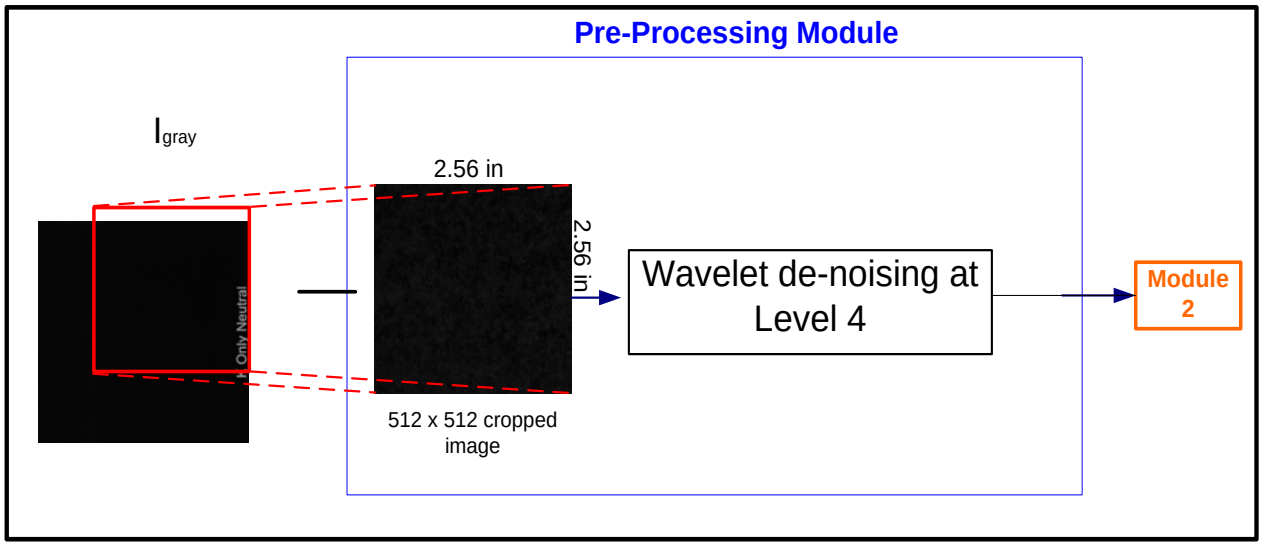

Figure 5: Detailed block diagram pre-processing module (M1)

The main function of this module is performed by what is known as "Wavelet De-noising". Wavelets have long been used in image compression and signal de-noising. Wavelet basis functions are spatially localized and give information of both scale and frequency. A brief mathematical description of this analysis is as follows.

2.2.1. Two dimensional Discrete Wavelet Transform (DWT) [33]

Images are 2-dimensional and are analyzed using a separable 2-D wavelet transform. A 2-D separable transform is equivalent to two 1-D transforms in series. It is

implemented as a 1-D row transform followed by a 1-D column transform on the data obtained from the row transform. Figure 6 shows the filter bank structure for computation of a 2-D DWT and IDWT.

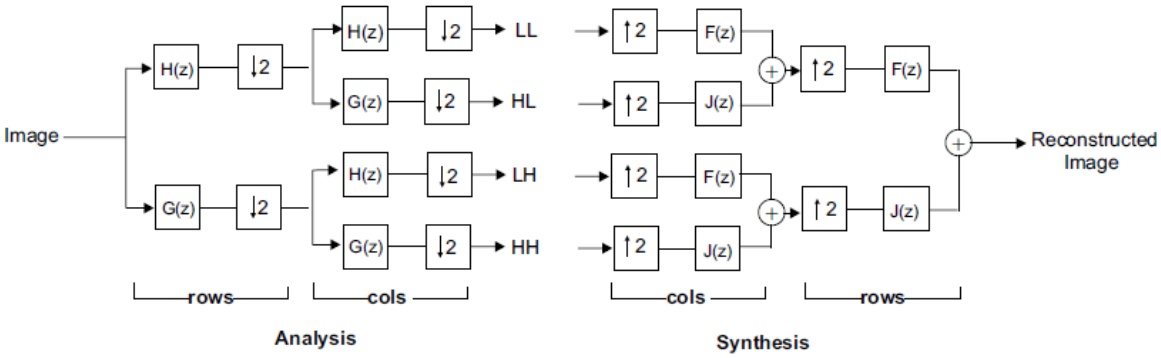

Figure 6: 2-D Wavelet analysis and synthesis with filter bank representation.

The separable 2-D basis functions can be expressed as the product of two 1-D basis functions. Unlike the 2 basis functions for 1-D signals at a given scale, there are four basis functions for 2-D signals as given in Eqn. (2)-(5).

$$\phi(u,v) = \phi(u)\phi(v) \tag{2}$$

$$\psi_1(u,v) = \psi(u)\phi(v) \tag{3}$$

$$\psi_2(u,v) = \phi(u)\psi(v) \tag{4}$$

$$\psi_3(u,v) = \psi(u)\psi(v) \tag{5}$$

$\phi(u,v)$ performs as the 2-D scaling function; whereas $\psi_1(u,v)$, $\psi_2(u,v)$ and $\psi_3(u,v)$ are the three 2-D wavelet functions. For a 2-D input signal $x(u,v)$, the transform coefficients are obtained by projecting the input onto the four basis functions given in Eqn. (2) – (5). These result in four different sub-bands in the decomposition corresponding to the four types of transform coefficients ($X(N, j, m), X^{(1)}(i, j, m), X^{(2)}(i, j, m)$ and $X^{(3)}(i, j, m)$). $X(N, j, m)$ is the coarse approximation of the 2-D signal $x(u,v)$ and corresponds to the

LL band. $X^{(1)}(i,j,m)$ coefficients contain the vertical details and correspond to the LH band. $X^{(2)}(i,j,m)$ coefficients contain the horizontal details and correspond to the HL sub-band. $X^{(3)}(i,j,m)$ coefficients represent the diagonal details in the image and constitute the HH sub-band. The four sub-bands for one level of decomposition are shown in Figure 7.

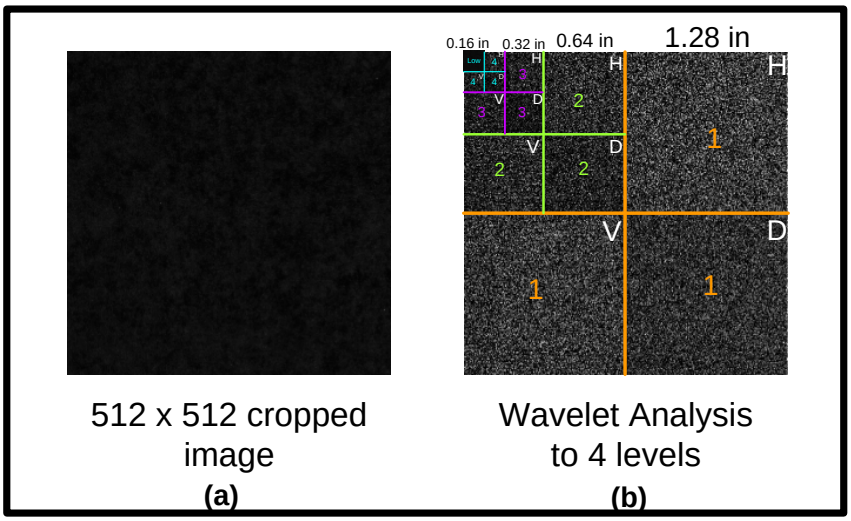

Figure 7: (a) Test image; (b) 4 sub-bands for a 4-Level Wavelet decomposition for one of the test images. Description: Low- LL level (white boundary-smallest square at Level 4); H: HL level (Horizontal), V: LH level (Vertical), D: HH level (Diagonal).

Thus, the 2-D DWT can be expressed as four inner products given by equations (6) – (9). As shown in Figure 6, it is computed by filtering each row in the image followed by filtering each column of the output obtained from the row filtering.

$$X(N,j,m) = \iint_{u,v} x(u,v)2^{N}\phi(2^{N}u-j)\phi(2^{N}v-m)dudv \tag{6}$$

$$X^{(1)}(i,j,m) = \iint_{u,v} x(u,v)2^{i}\psi(2^{i}u-j)\phi(2^{i}v-m)dudv \tag{7}$$

$$X^{(2)}(i,j,m) = \iint_{u,v} x(u,v)2^i \phi(2^i u - j)\psi(2^i v - m)dudv \tag{8}$$

$$X^{(3)}(i,j,m) = \iint_{u,v} x(u,v)2^i \psi(2^i u - j)\psi(2^i v - m)dudv \tag{9}$$

The above mentioned equations (6), (7), (8) and (9) represent the LL, LH, HL and HH sub-bands at level *i* respectively.

The synthesis stage corresponds to the 2-D IDWT or the Inverse Discrete Wavelet Transform given by Equation (10). The synthesis stage performs up-sampling and filtering in the reverse order (column followed by row filtering) to reconstruct the input image $x(u,v)$.

$$x(u,v) = \sum_j \sum_m X(N,j,m)2^N \phi(2^N u - j)\phi(2^N v - m)$$

$$+ \sum_i \sum_j \sum_m \begin{Bmatrix} X^{(1)}(i,j,m)2^i \psi(2^i u - j)\phi(2^i v - m) \\ + X^{(2)}(i,j,m)2^i \phi(2^i u - j)\psi(2^i v - m) \\ + X^{(3)}(i,j,m)2^i \psi(2^i u - j)\psi(2^i v - m) \end{Bmatrix} \tag{10}$$

Multiple levels of decomposition achieve higher de-correlation and are generated by iterating the LL output as shown in Figure 7. Note that the LL band is iteratively decomposed which results in a pyramid structure for the sub-bands with the coarsest sub-band at the top and the finest sub-band at the bottom.

The multi-resolution nature of the wavelet decomposition stores the energy in the signal into a small number of wavelet coefficients. For detailed images, much of the image energy is concentrated in the LL band that corresponds to the coarsest scale. The LL band is not only a coarse approximation of the image but also contains most of the image's energy. In addition to this, it is also statistically observed that the energy in the

inner sub-bands is also concentrated into a relatively small number of wavelet coefficients. The significant coefficients in the finer sub-bands do not occur at random, but rather tend to occur in clusters in the same relative spatial location in each of the higher frequency sub-bands. This self-similar, hierarchical nature of the wavelet transform can be used to make inter-band predictions; the location of the significant coefficients in the coarser bands is used to predict the location and magnitude of significant coefficients in inner sub-bands.

2.2.2. Wavelet De-noising

Here, we use a similar technique described by et al. [25] where the image is down-sampled using the discrete wavelet transform (DWT) analysis to 4 levels and all details (horizontal, vertical and diagonal) are completely removed (set to zero). This leaves only the approximation at level 4 or what we strictly call, the low frequency information. This approximation is then sent through a process of Wavelet synthesis (explained next) using the same filter banks employed in the aforementioned analysis procedure. This yields final reduced-noise image or what is also known as the *'perceptual approximation'*. The filter banks used for Wavelet analysis/synthesis are the same as used in JPEG2000 compression standard.

The down-sampling process is done until 4 levels. The primary reason behind choosing the number of levels = 4 is based on the fact that the human eye is governed by the Contrast Sensitivity Function (CSF) [26]. The peak of the chosen CSF (explained in Section 2.3) occurs at a spatial frequency of 6.25 cycles/inch, this corresponds to a wavelength, $\lambda = 0.16$ inches or a scale of 32x32 pixels in the wavelet domain. Our input image, after being converted to grayscale and cropped to a size of 512x512 pixels is sent

through the wavelet de-noising procedure. Thus, as described above, all high frequency horizontal, vertical and diagonal details denoted as H, V and D respectively, are removed and a de-noised image of resolution 512x512 pixels is synthesized or reconstructed using Eqn. 10. The complete pre-processing pipeline is explained in Figure 8.

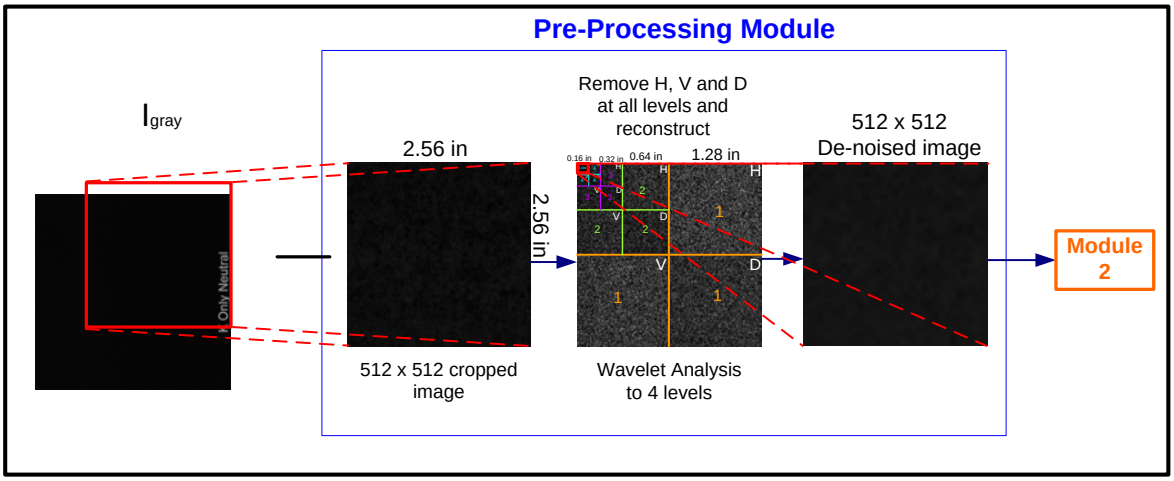

(a)

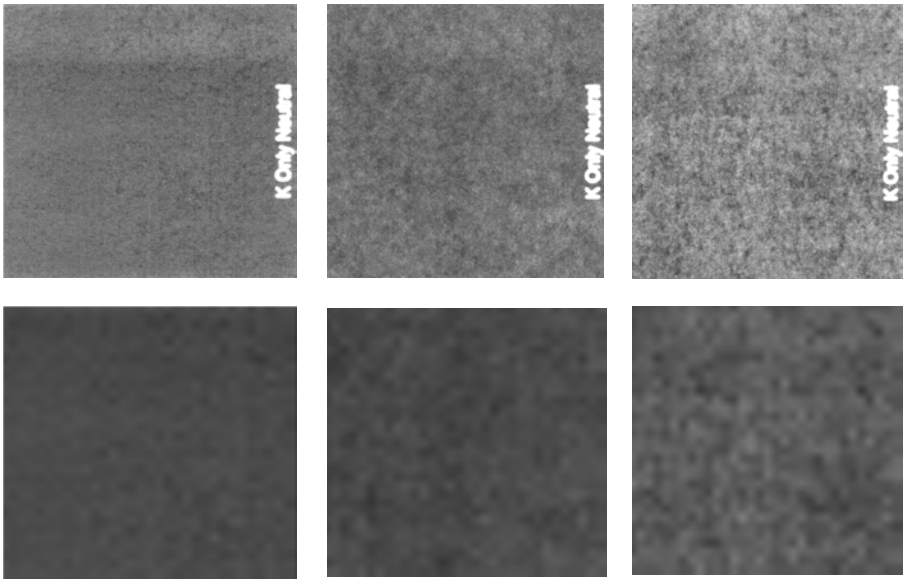

(b)

Figure 8: Pre-processing module: (a) Block diagram of Module 1; (b) Contrast enhanced Test samples (Top row) and the corresponding de-noised outputs from the pre-processing module (Bottom row).

2.3 Contrast Sensitivity Function (CSF)

Human Visual System (HVS) models have been widely used in the variety of applications in image processing and image quality assessment [26]. One of the aims of this thesis was to develop a stable visual system to evaluate print defects of a particular class, known as mottle. Hence, it becomes necessary to look into all possible models that characterize the HVS.

To serve the purpose of our application, we implemented 5 HVS models. We have used only one of them in the algorithm based on the peak sensitivity and the corresponding spatial frequency. Kim *et al.* [26] explained the impact of different HVS models on halftoning along with detailed implementation description of different model. Campbell *et al.* [27] proposed and developed a HVS model by measuring the contrast threshold for detecting sinusoidal interference fringes generated by an oscilloscope at a viewing distance of 57 inches. It achieves a maximum at a spatial frequency ~6.25 cycles/inch (cpi). The second model implemented for our study was proposed by Mannos and Sakrison [28]. They performed subjective tests on images that were coded with optimal parameters using the model. The resulting CSF peaked at 7.9 cpi. The third model that has been implemented was proposed by Näsänen [29] which primarily replicates a low pass filter characteristic. Hence, the maximum for this CSF occurs at 0 cpi. Daly's model [30] also has a low pass characteristic, this model is same as the one proposed by Mannos *et al.* but with different parameters. The maximum of this CSF occurred at 6.6 cpi. The most general model proposed by Barten [31] is the most widely used and can be matched with all the other models above by adjusting this model's

parameters. There are no parameter sets that were included in [30] which generates different model than the ones already mentioned.

We use the Campbell's CSF in our proposed algorithm as it peaks at a spatial frequency which corresponds to the scale (32x32 pixels and 0.16x0.16 in^2) of level 4, hence, performing a low pass filtering operation in the wavelet domain as just like the HVS.

As described above, five CSF models were implemented (see Figure 9) along with a model provided by Hewlett Packard Company for experimental purposes. The radial frequency axes for the CSF are implicitly generated by making use of the sampling theorem. The size of the image and the scanning resolution (sampling frequency) are set at 512x512 pixels and 200 dpi respectively. Our purpose in using the CSF is to simulate the behavior of the HVS to compute one of the features in frequency domain.

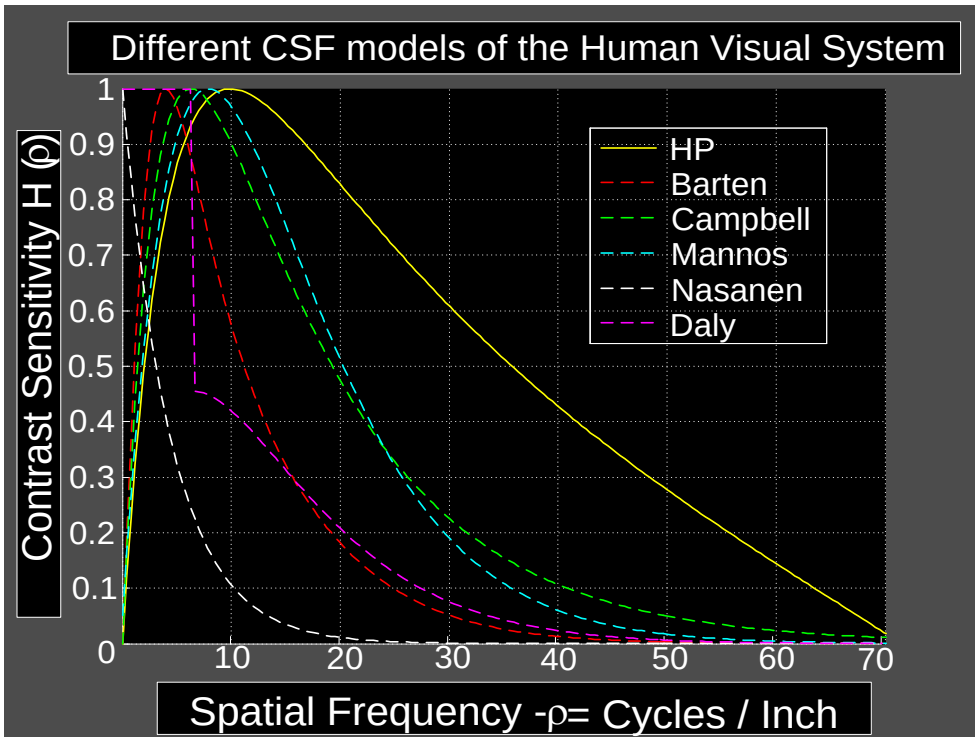

Figure 9: Different 1-D CSF curves implemented originally in 2D for filtering.

2.4 Spatio-Frequency Parameter Estimation (M2)

The parameter estimation module comprises of 2 major sub-modules. One evaluates parameters (alternatively referred as features) strictly in the frequency domain, and the other computes features in the spatial domain. These two sub-modules and the corresponding mottle features are explained in sections 2.3.1 and 2.3.2 respectively.

In this thesis, the amount of print mottle is evaluated using the information stored in the samples' spatial frequency and spatial distribution. These two characteristics can be further described or measured in context of print mottle by different features or measures in the frequency domain as well as the spatial domain. For this work, we computed 2 frequency domain features and 9 spatial domain features. The frequency features are computed by transferring the image to the Fourier domain using the Fast Fourier Transform algorithm [32]. A block diagram depicting the features in both domains is shown in Figure 10.

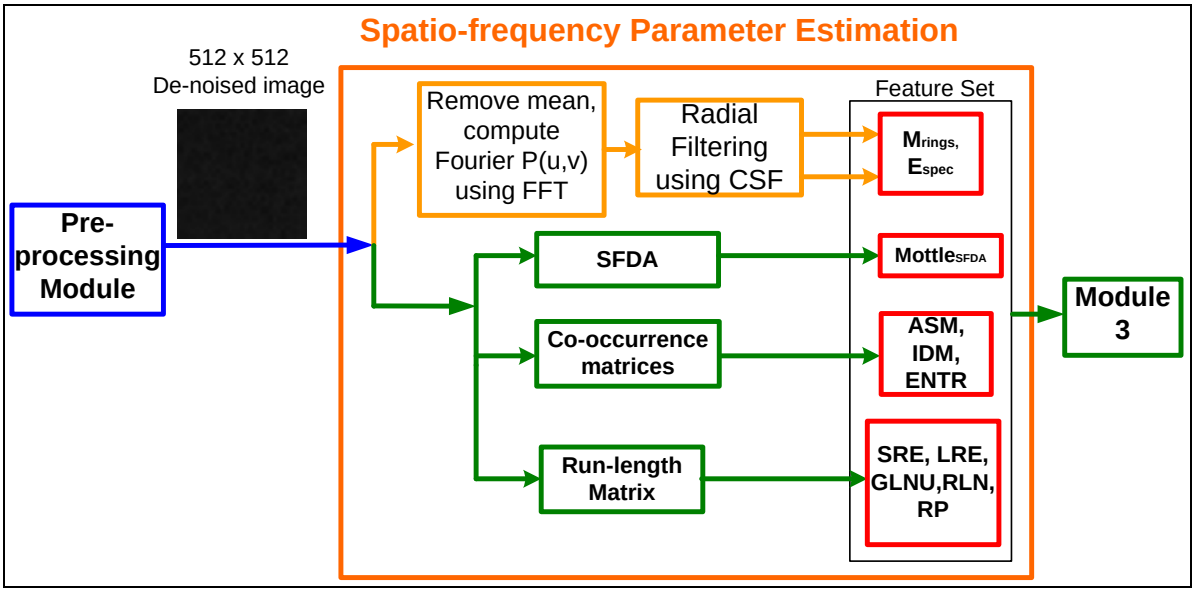

Figure 10: Detailed block diagram of Module 2: Spatio-frequency parameter estimation.

2.4.1. Frequency Domain Features

As mentioned previously, the initial objective is to compute features that give a measure of variation across the test target.

A 2-D Fast Fourier Transform (FFT) of the 512 x 512 test image generated at the end of the pre-processing stage is computed and the subsequent power spectrum (Squared Magnitude) is calculated. We subtract the mean of the image before taking the FFT for the purpose of normalization. The effects due to banding and streaking are also eliminated by setting the first row and column of the power spectrum to zero. An example of a power spectrum is shown in Figure 11(a). To re-iterate the effect of removing streaks and banding, Figure 11(b) is a magnified version of Figure 11(a). Note that high frequency content was already removed in the pre-processing module by means of wavelet domain de-noising. Hence, there is high presence of low frequency content.

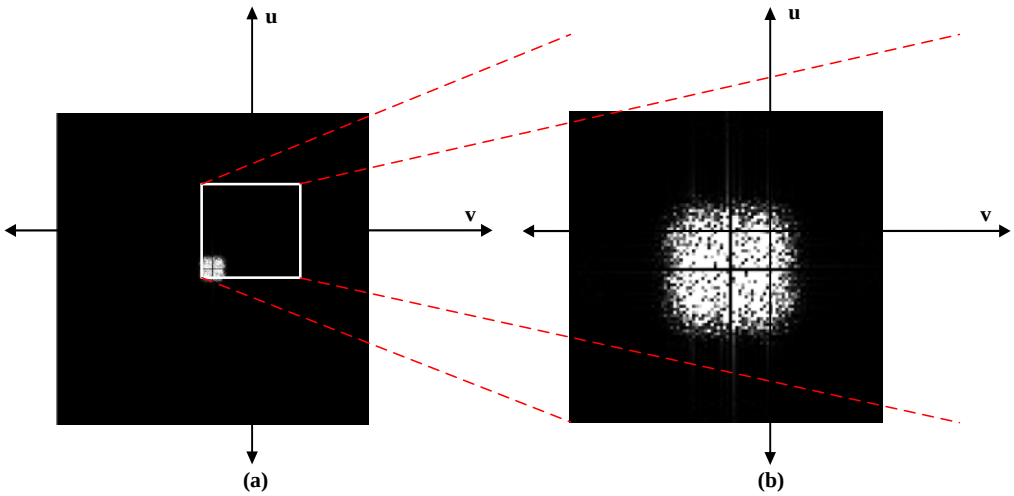

Figure 11: (a) 2-D Power Spectrum of 'perceptual approximation'; (b) cropped version of (a) to re-iterate the absence of any high frequency content and effects due to streaking and banding.

Consequently, the power spectrum can now be used to compute the following two features: 1) Ring Mottle (M_{rings}); 2) Spectral Entropy (E_{spec}). To compute M_{rings}, we make use of a technique known as 'radial filtering'. It can clearly be seen from Figure 11 that the power spectrum contains only low frequency content. To perform 'radial filtering', we define radial frequency bands as Binary Radial Band Maps (BRBMs) which are each multiplied with the power spectrum and subsequently pixel values are added providing energy in each band. BRBM start from the center with a radial width of 1 pixel corresponding to the lowest radial frequency. This width may be increased in steps of 1, 2, 3, 4, 5 and 10 pixels depending on the user's requirements. A pseudo-color representation of these BRBMs together is shown in Figure 12.

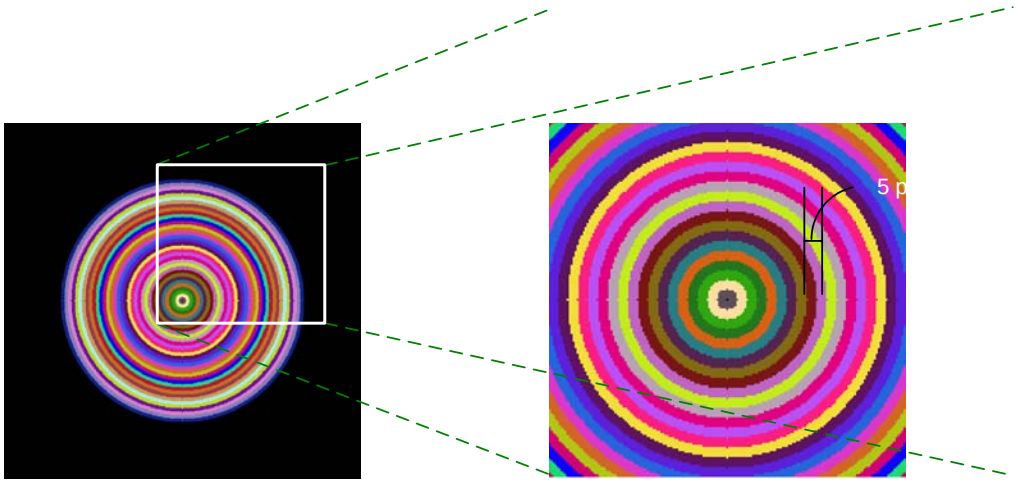

Figure 12: (a) BRBM (5 pixels width) in image dimensions; (b) BRBM corresponding to low frequency content.

BRBMs are multiplied with the image, to demonstrate the phenomenon of frequency domain filtering, subsequently giving energy (measure of variation) in each band. Shown in Fig. 7 is the work flow to compute M_{rings}. The discrete power spectrum *P (u, v)* of an N

x N image where *u* and *v* represent frequencies along the X-direction and Y-direction respectively (see Figure 11), is multiplied point-by-point with the Contrast Sensitivity Function (CSF) described in Section 2.2 resulting in a filtered signal that depicts the HVS response. The expression for uniformity in each band is given below:

$$U_i = \sum_{u=1}^{N}\sum_{v=1}^{N}\left[P(u,v)C(u,v)\right]H_i(u,v) \tag{11}$$

where, *C (u, v)* is the CSF (Fig. 4), H_i(u, v) is BRBM of i^{th} frequency band (Fig. 6) and U_i gives the energy in the i^{th} frequency band. Consequently, the Ring Mottle (M_{rings}) is computed utilizing the aforementioned uniformity in each band (Eqn. 12):

$$M_{rings} = \sum_{i=1}^{f_0} U_i \Big/ N \tag{12}$$

where, $f_0 = \sqrt{u^2 + v^2} \leq 70$ cycles/inch (HVS response ~ 0) and FFT Size, N = 512.

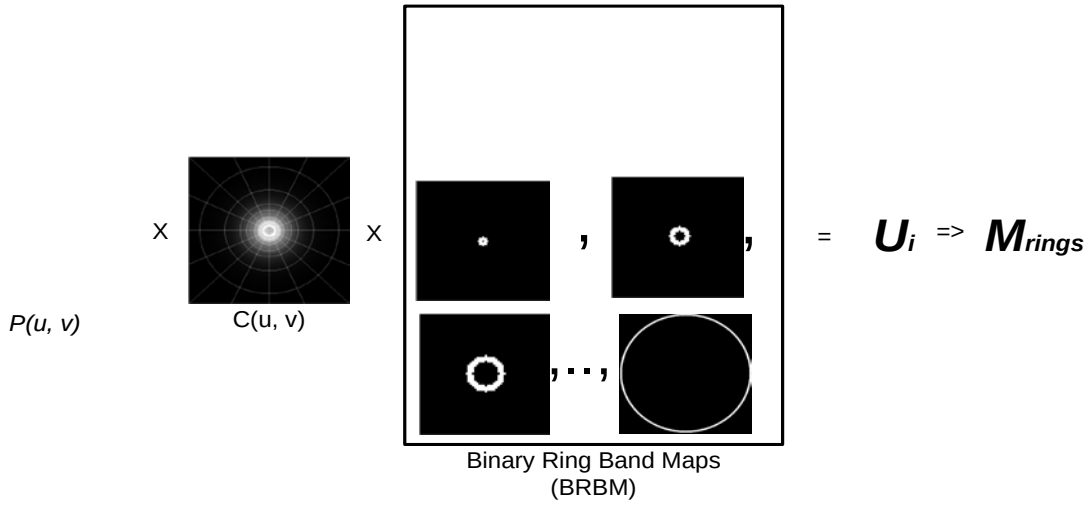

Figure 13: Flow for calculation of Ring Mottle (M_{rings}).

The values for M_{rings} of 10 test targets are summarized in Chapter 4. The next feature computed is the Spectral Entropy (E_{spec}), using the probability distribution of the power spectrum P (u, v). The following expression is used for computing E_{spec}:

$$E_{spec} = -\sum_{u=1}^{N}\sum_{v=1}^{N} \Pr(u,v)\log_2\{\Pr(u,v)\} \quad (13)$$

$$\text{where,} \quad \Pr(u,v) = P(u,v) \Big/ \sum_{u,v} P(u,v)$$

is the probability distribution of *P (u, v)*. When the texture of the discrete power spectrum is more random, all $\Pr(u,v)$ values are significantly high, yielding large entropy values and vice versa. This implies, a highly irregular pattern needs more information to be described, hence has a high entropy. The values of spectral entropy for our 10 test targets are summarized in Table 1. Note that, spectral entropy is not calculated using the ring-shaped masks, but over the whole power spectrum (Figure 11).

Once these features are calculated for the current target, the proposed algorithm proceeds to spatial domain analysis, explained in next section, consequently providing a parallel nature of computation to the algorithm, in multiple domains.

2.4.2 Spatial Domain Analysis

The motive behind exploring the spatial domain is the flexibility provided by various tools such as first and second order statistics using the co-occurrence (CO) matrices of size L x L (depending on the dynamic range of the image). CO matrices are calculated in 4 directions (0^o, 180^o, 90^o and -90^o) represented in Figure 14 below and then cumulated together to give one CO matrix.

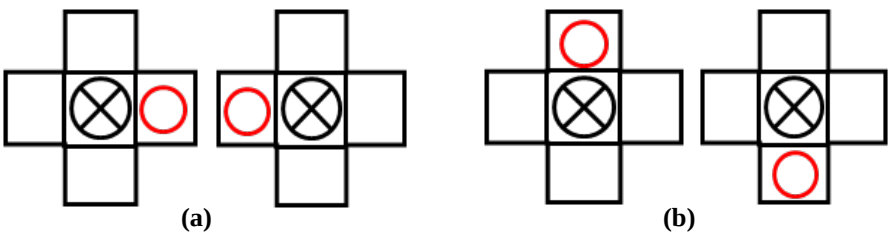

Figure 14: Directional setting for Co-occurrence matrix (a) 0^o and 180^o; (b) 90^o and -90^o.

After the final CO matrix is obtained, a set of pre-selected features is calculated. These features include Angular Second Moment (ASM), Inverse Difference Moment (IDM), and Spatial Entropy (ENTR) [33]. The following three equations summarize the above mentioned features.

$$ASM = \sum_{m=0}^{N-1}\sum_{n=0}^{N-1}\left[P(m,n)\right]^2 \tag{14}$$

$$IDM = \sum_{m=0}^{N-1}\sum_{n=0}^{N-1} P(m,n) \Big/ \left[1+(m-n)^2\right] \tag{15}$$

$$ENTR = -\sum_{m=0}^{N-1}\sum_{n=0}^{N-1} P(m,n)\log_2[P(m,n)] \tag{16}$$

ASM corresponds to amount of orderliness in the target. Orderliness measures how uniform are the pixel values in a window. If the texture is extremely random or the variation is high, the value of ASM is low and vice versa. Same is the case for IDM. Hence, these values are sorted in descending order to be in accordance with the ranking algorithm which works on the principle of lowest to highest (Best to Worst). IDM has smaller numbers for images with high contrast, larger numbers for images with low contrast. The values for three features from 10 test targets are summarized in Table 1.

Another set of spatial features based on gray level run lengths is used here. A gray level run is a set of consecutive pixels having the same gray level value. Run Length Matrices (RLM) are described in [33]: RLM_{0^0} and RLM_{90^0} are calculated and subsequently 5 features are computed from each of them (see Eqns. (17) – (21)). Run length features represent the textural information related to the number of times each gray level appears. A simple 4x4 image is shown in Figure 15 to demonstrate the computation of RLM in detail.

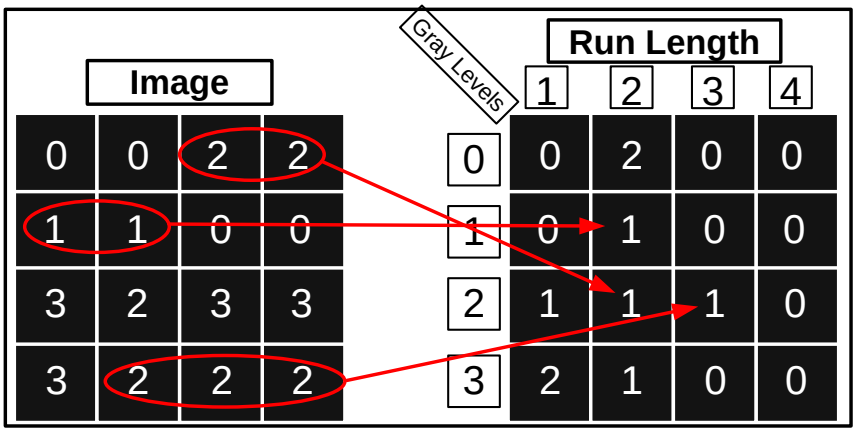

Figure 15: A sample 4x4 image (4 gray levels) with its corresponding Run Length Matrix RLM_0.

Subsequently, all features from the two RLMs (5 from each) are averaged to obtain the final set of features to be incorporated in the metric. The five features are: (1) Short Run Emphasis (SRE); (2) Long Run Emphasis (LRE); (3) Gray Level Non-uniformity (GLNU); (4) Run Length Non-uniformity (RLNU); (5) Run Percentage (RP). These features [33] are mathematically given by Eqn. (17) – (21):

$$SRE = \sum_{i=0}^{N_g}\sum_{j=1}^{N_r} Q_{RL}(i,j)/j^2 \Big/ \sum_{i=0}^{N_g}\sum_{j=1}^{N_r} Q_{RL}(i,j) \tag{17}$$

$$LRE = \sum_{i=0}^{N_g}\sum_{j=1}^{N_r} j^2 Q_{RL}(i,j) \Big/ \sum_{i=0}^{N_g}\sum_{j=1}^{N_r} Q_{RL}(i,j) \tag{18}$$

$$GLNU = \sum_{i=0}^{N_g}\left[\sum_{j=1}^{N_r} Q_{RL}(i,j)\right]^2 \Big/ \sum_{i=0}^{N_g}\sum_{j=1}^{N_r} Q_{RL}(i,j) \tag{19}$$

$$RLN = \sum_{j=1}^{N_r}\left[\sum_{i=0}^{N_g} Q_{RL}(i,j)\right]^2 \Big/ \sum_{i=0}^{N_g}\sum_{j=1}^{N_r} Q_{RL}(i,j) \tag{20}$$

$$RP = \sum_{i=0}^{N_g}\sum_{j=1}^{N_r} Q_{RL}(i,j) \Big/ L \tag{21}$$

These 5 features were picked because they provide a good range of measures for textures with long-scale variations, also known as macro-textures serving the purpose of their incorporation into the algorithm. Each feature has its own significance: SRE represents the shorter runs of non-uniformity. LRE signifies longer runs of non-uniformity. GLNU takes small values when the runs are uniformity distributed among gray levels. The fourth feature, RLNU takes small values when gray levels are uniformly distributed among run-lengths. Lastly, RP represents the average runs per pixel and takes small values for smooth and less mottled images.

Another spatial feature included in our feature set, described by Rosenberger [34] is known as the Spatial Frequency Distribution Analysis (SFDA). The motive behind using this analysis is that it adds a feature based on local variation information to the final feature set. Also, originally this feature is intended to compute the amount of graininess in a target, but we modified it to provide us with a measure of mottle in the target. A formula different from [34] is used in our metric.

In any digital image which consists of low frequency gray level variation, the SFDA algorithm proposed [34] measures the two dimensional rate of change in luminance values and transitions between light and dark throughout the image. Many parameters affect our visual system as described in [34]. To corroborate this fact, the author states - “The human visual system operates in a three dimensional environment (Subjective Analysis setup) composed of the luminance intensities governed by parameters like length and height of the viewing area relative to the observer’s visual system”. SFDA extracts square contiguous target areas of the same pixel dimensions in an iterative fashion, as shown in Figure 16 below:

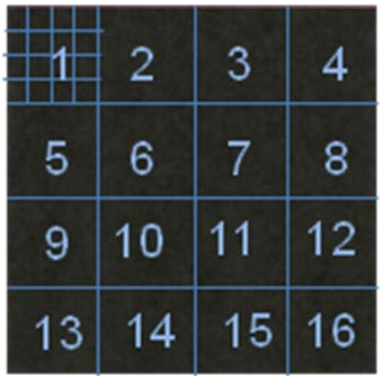

Figure 16: Spatial Distribution: A typical target size (512x512) composed of 16 128x128 targets.

A rather different metric than SFDA is used here, but is not named differently. The 16 sub-targets labeled in Figure 16 are further sub-divided into 16 targets each of size 32 x 32 pixels (See Figure 17). The bigger targets are exactly of size 128x128. As mentioned in Section 2.1, the scale of 32 x 32 corresponds to a frequency which is in correspondence with the peak visual response of the human eye making it a consistent observation. These measurements are made on 'perceptual approximation' obtained using wavelet de-noising (explained before).

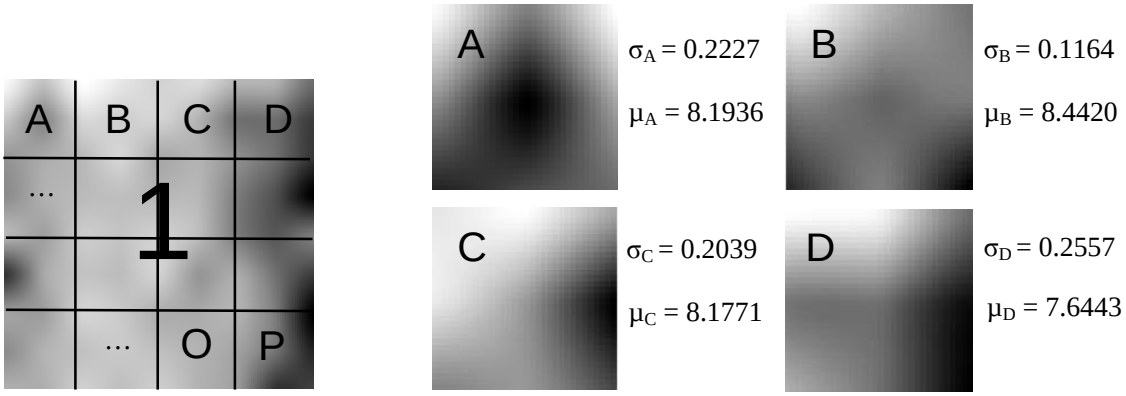

Figure 17: Spatial distribution of sub-target no. 1 shown in Fig. 16; (a) 4x4 grid shown on large 128x128 target; (b) expanded view of first 4 sub-targets in (a).

In Figure 17, $\sigma_A, \ldots, \sigma_D$ are the standard deviation values and μ_A are the mean values for each 32x32 sub-target. As seen from Fig. 10, sub-target B has a lower value of σ as it's more uniform in appearance as compared to the other 3 sub-targets. Also, the appearance of these sub-targets is contrast-based making them appear lighter as all pixels have value between 0 and 10 on a scale of 255.

If we calculate the above mentioned values for all small 32x32 sub-targets, it yields 2 vectors, one is $\alpha_i = [\sigma_A, \sigma_B, \sigma_C, \sigma_D, \sigma_E, \ldots\ldots, \sigma_P]$ and the other is the Mean vector $\beta_i = [\mu_A, \mu_B, \mu_C, \mu_D, \mu_E, \ldots\ldots, \mu_P]$ where $i = 1, 2, \ldots, 16$. We compute 3 attributes using the above two vectors to facilitate the final computation of mottle. These are known as μ_i (Mean of α_i), σ_i (standard deviation of α_i) and $\mu_{\beta i}$ (Mean of β_i). The target mean, $\mu_{\beta i}$ is a good indicator of the diversity of visual intensities or local area contrasts. Next we compute, what is called the Local Mottle for each 128x128 sub-target and is expressed mathematically as:

$$M_{(i),Local} = \mu_i \sigma_i \mu_{\beta i} \tag{22}$$

where, $M_{(i),Local}$ represents the mottle for each 128x128 sub-target. This process, when carried out for all 16 sub-targets, gives us a vector which consists of local mottle values.

This expression is different from the one proposed by [34] in the sense that original SFDA uses the standard deviation of β_i rather than the mean. The reason behind this change is that the degree of variation amongst α_i is a measure of uniformity in the small 128x128 sub-targets and the mean $\mu_{\beta i}$ acts as a local scaling factor for that particular sub-target. The mean of the standard deviations, μ_i of smaller 32x32 sub-targets gives an average variation inside that 128x128 sub-target. These 3 factors, when multiplied

together provide a good local variation estimate. Final SFDA mottle value is expressed as a product of standard deviation of $M_{(i),\,Local}$ and its mean (see Eqn. 23).

$$Mottle_{SFDA} = \sigma_{M_i} \mu_{M_i} \tag{23}$$

where, σ_{Mi} and μ_{Mi} are the standard deviation and mean for local mottle values computed in Eqn. 13. The proposed change in the existing algorithm results in a better co-relation with the subjective rankings. The values for 10 test targets of SFDA mottle are summarized in Table 1 along with other features.

The parameters given by Eqns. (14) – (21) and (23) give the 9 features that comprise the final value of SFMM. To summarize, we provide a high-level block diagram for overall parameter estimation in Figure 10 provided at the beginning of Section 2.4.

2.5 Ranking Algorithm

After obtaining all features (attributes) from Module 2 for all 10 test targets, the data is organized in form of vectors. These vectors are further normalized with respect to the local maximum value. This is done to limit the maximum SFMM value to number of features. Next, the normalized parameters are obtained in form of a matrix of size M x N where M equals number of test targets (10) and N is the number of features (11) known as the Feature Value Matrix (FVM). A tabulated version of FVM for 10 targets out of the numerous test samples is given in Table 1 for the ease of understanding of this section.

Test Target	Printer	Media	Ring Mottle	Spec. Entropy	ASM	IDM	ENTR	SFDA	SRE	LRE	GLNU	RLN	RP
1	1	Canon Color Laser	0.06	0.97	0.91	0.06	0.39	0.00	0.74	0.21	0.34	0.08	0.27
2	1	Hammermill Fore	0.11	1.00	0.84	0.22	0.05	0.03	0.71	0.55	0.64	0.15	0.36
3	1	Hammermill Laser	0.17	0.93	0.92	0.22	0.34	0.01	0.51	0.77	0.65	0.16	0.41
4	1	Xerox Bus. 4200	0.51	0.97	0.95	0.21	0.62	0.13	0.76	0.97	0.97	0.54	0.75
5	2	Canon Color Laser	0.11	0.97	0.90	0.26	0.19	0.01	0.55	0.76	0.75	0.16	0.41
6	2	Hammermill Laser	0.40	0.95	0.94	0.25	0.53	0.06	0.65	0.92	0.79	0.31	0.58
7	2	Xerox Bus. 4200	0.70	0.96	0.97	0.31	0.75	0.21	0.77	0.97	0.91	0.55	0.76
8	3	Canon Color Laser	0.15	0.98	0.93	0.20	0.44	0.02	0.59	0.81	0.64	0.18	0.44
9	3	Hammermill Laser	0.47	0.94	0.97	0.27	0.73	0.15	0.76	0.95	0.79	0.42	0.67
10	3	Xerox Bus. 4200	1.00	0.97	1.00	1.00	1.00	1.00	1.00	1.00	1.00	1.00	1.00

Table 1: Feature Value Matrix for 10 K only Test Targets.

Note that the numerical values in Table 1 are normalized. Prior to normalization, these values were weighted using empirical log-weights. Section 2.5.1 below gives a brief introduction to the weighting scheme and subsequently the normalization scheme applied to the true feature values.

2.5.1. Weighting and Normalization of Features

Due to the nature and intensity values of these samples, the feature values acquire values that different across each feature but consistent along sample. Out final objective is to come up with one numerical value that signifies mottle in these samples, hence we need

to get these features to the same scale and hence normalize them. The first step is to eliminate any exponent powers acquired by these features and bring them to a scale between 1 and 10. This is done by the following set of equations:

$$\mu_{Raw} = \sum_{i=1toN} f_i \Big/ N \tag{24}$$

$$W_{feature} = 10^{-(\Omega[\log_{10}(\mu_{raw})])} \tag{25}$$

where, $\Omega(x) = round(x)$ rounds off x to the nearest integer

The weights are computed for each feature, and further normalized along each feature using the maximum value and brought to a scale of 0 to 1. The following set of tables give a brief overview of features and their weighted and normalized values.

Test Target	Printer	Media	Ring Mottle	Spec. Entropy	ASM	IDM	ENTR	SFDA	SRE	LRE	GLNU	RLN	RP
1	1	Canon Color Laser	0.07	6.58	1.80	0.08	1.16	0.00	0.02	7959.48	1463.85	59.67	0.02
2	1	Hammermill Fore	0.12	6.82	2.37	0.02	0.14	0.02	0.02	4660.98	2775.90	108.07	0.02
3	1	Hammermill Laser	0.19	6.34	1.67	0.02	1.04	0.01	0.01	2621.02	2818.75	119.98	0.03
4	1	Xerox Bus. 4200	0.58	6.62	1.39	0.02	1.87	0.10	0.02	696.87	4190.66	397.43	0.05
5	2	Canon Color Laser	0.13	6.63	1.86	0.02	0.56	0.01	0.01	2714.67	3250.15	115.24	0.03
6	2	Hammermill Laser	0.46	6.49	1.49	0.02	1.59	0.04	0.02	1173.33	3422.95	225.58	0.04
7	2	Xerox Bus. 4200	0.80	6.51	1.22	0.02	2.24	0.15	0.02	677.50	3933.94	406.38	0.05
8	3	Canon Color Laser	0.18	6.65	1.57	0.03	1.32	0.01	0.02	2226.79	2774.58	130.46	0.03
9	3	Hammermill Laser	0.54	6.41	1.26	0.02	2.19	0.11	0.02	894.24	3405.38	312.86	0.05
10	3	Xerox Bus. 4200	1.15	6.59	0.96	0.01	3.00	0.74	0.03	379.88	4330.83	737.99	0.07

(a)

Test Target	Printer	Media	Ring Mottle	Spec. Entropy	ASM	IDM	ENTR	SFDA	SRE	LRE	GLNU	RLN	RP
1	1	Canon Color Laser	0.07	6.58	0.82	0.08	1.16	0.00	0.02	2.04	1.46	0.60	0.02
2	1	Hammermill Fore	0.12	6.82	0.76	0.02	0.14	0.02	0.02	5.34	2.78	1.08	0.02
3	1	Hammermill Laser	0.19	6.34	0.83	0.02	1.04	0.01	0.01	7.38	2.82	1.20	0.03
4	1	Xerox Bus. 4200	0.58	6.62	0.86	0.02	1.87	0.10	0.02	9.30	4.19	3.97	0.05
5	2	Canon Color Laser	0.13	6.63	0.81	0.02	0.56	0.01	0.01	7.29	3.25	1.15	0.03
6	2	Hammermill Laser	0.46	6.49	0.85	0.02	1.59	0.04	0.02	8.83	3.42	2.26	0.04
7	2	Xerox Bus. 4200	0.80	6.51	0.88	0.02	2.24	0.15	0.02	9.32	3.93	4.06	0.05
8	3	Canon Color Laser	0.18	6.65	0.84	0.03	1.32	0.01	0.02	7.77	2.77	1.30	0.03
9	3	Hammermill Laser	0.54	6.41	0.87	0.02	2.19	0.11	0.02	9.11	3.41	3.13	0.05
10	3	Xerox Bus. 4200	1.15	6.59	0.90	0.01	3.00	0.74	0.03	9.62	4.33	7.38	0.07

(b)

Test Target	Printer	Media	Ring Mottle	Spec. Entropy	ASM	IDM	ENTR	SFDA	SRE	LRE	GLNU	RLN	RP
1	1	Canon Color Laser	0.06	0.97	0.91	1.00	0.39	0.00	0.74	0.21	0.34	0.08	0.27
2	1	Hammermill Fore	0.11	1.00	0.84	0.26	0.05	0.03	0.71	0.55	0.64	0.15	0.36
3	1	Hammermill Laser	0.17	0.93	0.92	0.25	0.34	0.01	0.51	0.77	0.65	0.16	0.41
4	1	Xerox Bus. 4200	0.51	0.97	0.95	0.27	0.62	0.13	0.76	0.97	0.97	0.54	0.75
5	2	Canon Color Laser	0.11	0.97	0.90	0.22	0.19	0.01	0.55	0.76	0.75	0.16	0.41
6	2	Hammermill Laser	0.40	0.95	0.94	0.22	0.53	0.06	0.65	0.92	0.79	0.31	0.58
7	2	Xerox Bus. 4200	0.70	0.96	0.97	0.20	0.75	0.21	0.77	0.97	0.91	0.55	0.76
8	3	Canon Color Laser	0.15	0.98	0.93	0.31	0.44	0.02	0.59	0.81	0.64	0.18	0.44
9	3	Hammermill Laser	0.47	0.94	0.97	0.21	0.73	0.15	0.76	0.95	0.79	0.42	0.67
10	3	Xerox Bus. 4200	1.00	0.97	1.00	0.06	1.00	1.00	1.00	1.00	1.00	1.00	1.00

(c)

Table 2: Results from 10 test targets: (a) Raw Feature values (f_i), (b) Weighted feature values, (c) Normalized and Weighted feature values (FVM).

The final weighted and normalized values are shown in Table 2(c). This table is known as the Feature Value Matrix (FVM) which is used for a priori ranking process explained in the following section.

2.5.2. Cumulative Ranking (*a priori* ranking)

The *a priori* ranking is obtained by arranging most of the features in ascending order, although this is not the case with ASM, IDM and SRE which are ranked in descending order to maintain the consistency with other 8 features. FVM is ranked along columns and resulting matrix is known as the Feature Rank Matrix (FRM). The FRM is shown in Table 3(a). In each column of FRM, rank 1 corresponds to the "Best sample" and 10 correspond to the "Worst Sample". Rankings can be compared along columns, each target contains a majority rank which has the highest frequency of occurrence and is known as the Cumulative Rank (CR). For our testing purposes, we implemented two methods of obtaining the cumulative rankings. One method is mode-based (Section 2.4.2.1) and the other method is weight-based (Section 2.4.2.2) as explained in the following two sections.

2.5.2.1. Mode-based method

In this ranking process, n test targets are ranked in *r* different rankings according to 7 features. A vote count V_{ir} is evaluated in the i^{th} test target for r^{th} rank, resulting in a vote vector called the $\boldsymbol{V_i}$. The maximum value in $\boldsymbol{V_i}$ is searched for and the index corresponding to this value is given as the rank for the corresponding test target. For example, if test target 1 has been voted 4 times as rank = 1, then clearly the maximum value in $\boldsymbol{V_i}$ would be V_{11} = 4 where 1 is the cumulative rank (CR) for this target (See Table 3 and Eqn. 26). The process is repeated for all targets.

$$CR_i = r \text{ if } \quad V_{ir} = \max(\boldsymbol{V_i}) \tag{26}$$

Test Target	Ring Mottle	Spec. Entropy	ASM	IDM	ENTR	SFDA	SRE	LRE	GLNU	RLN	RP	Cumulative Rank
1	1	5	3	10	4	1	6	1	1	1	1	**1**
2	2	10	1	7	1	5	5	2	3	2	2	**2**
3	5	1	4	6	3	3	1	4	4	4	4	**4**
4	8	7	7	8	7	7	8	8	9	8	8	**8**
5	3	8	2	4	2	2	2	3	5	3	3	**3**
6	6	3	6	5	6	6	4	6	7	6	6	**6**
7	9	4	9	2	9	9	9	9	8	9	9	**9**
8	4	9	5	9	5	4	3	5	2	5	5	**5**
9	7	2	8	3	8	8	7	7	6	7	7	**7**
10	10	6	10	1	10	10	10	10	10	10	10	**10**

Table 3: FRM for 10 test targets (‘1’ = Least Mottle; ….‘10’=Most Mottle) using the Mode-based method.

There are ranks along each row which are considered as insignificant features. For example, if seven features rank a target as ‘1’ and the remaining four features rank it 5 and 6, then these two features would be considered as insignificant features as they completely disagree with the consensus as well as the Cumulative ranks. This process can be corresponded to linear regression followed by elimination of outliers for better understanding.

2.5.2.1. Weight-based method

Given 10 test targets, these are ranked in *r* different rankings according to *m* features. First, a sum of rank values is computed using the following expression:

$$S_i = \sum_{k=1}^{n} f_{ik} R_k \tag{27}$$

Where *i* represent the i^{th} image and vary from 1 to 10. The index *k* gives the rank that varies from 1 to 10. The term f_{ik} represents the number of features that give the i^{th} image a rank *k*. The term R_k is a vector in the reverse order to *k* and is given by $R_k = n - k + 1$. Finally, these values of S_i are arranged in descending order and the indices corresponding to this order are given as ranks to the images corresponding to *i*. The rankings from this method are presented in Table 4. The final ranking obtained is known as the Cumulative Rankings (CR) vector.

Test Target	Ring Mottle	Spec. Entropy	ASM	IDM	ENTR	SFDA	SRE	LRE	GLNU	RLN	RP	Cumulative Rank
1	1	5	3	10	4	1	6	1	1	1	1	**1**
2	2	10	1	7	1	5	5	2	3	2	2	**2**
3	5	1	4	6	3	3	1	4	4	4	4	**4**
4	8	7	7	8	7	7	8	8	9	8	8	**8**
5	3	8	2	4	2	2	2	3	5	3	3	**2**
6	6	3	6	5	6	6	4	6	7	6	6	**6**
7	9	4	9	2	9	9	9	9	8	9	9	**9**
8	4	9	5	9	5	4	3	5	2	5	5	**5**
9	7	2	8	3	8	8	7	7	6	7	7	**7**
10	10	6	10	1	10	10	10	10	10	10	10	**10**

Table 4: FRM for 10 test targets (‘1’ = Least Mottle; …. ‘10’=Most Mottle) using the Weight-based method.

Conclusively, any of the two methods can be used here for ranking as the difference between the two Cumulative rankings is not large for the two respective methods. Hence, either of the two methods can be used. These ranking matrices are used for the next stage

of the algorithm i.e. Insignificant Feature Removal Stage (IFRS) explained in Section 2.4. The final metric is computed after the insignificant features are removed.

2.6 Insignificant Feature Removal Stage

This part of the algorithm removes the insignificant features using a maximum correlation based criterion between each feature rank and the CR obtained previously from maximum voting. The last row in Table 5 gives the correlation between CR and corresponding feature ranks. The criterion for removing the insignificant features is a correlation threshold. If the correlation between CR (also known as apriori ranks) and the rank of the corresponding feature is less than 80%, it is declared as an insignificant feature. This value is fixed at 80% fulfilling the level of accuracy we require initially and is still not a final threshold value. The columns for insignificant features are set to 0 in the FVM (See Table 2(c)). Depending on the color of the test target and the amount of variation, the eliminated features may vary.

Test Target	Ring Mottle	Spec. Entropy	ASM	IDM	ENTR	SFDA	SRE	LRE	GLNU	RLN	RP	Cumulative Rank
1	1	5	3	1	4	1	6	1	1	1	1	**1**
2	2	10	1	4	1	5	5	2	3	2	2	**2**
3	5	1	4	5	3	3	1	4	4	4	4	**4**
4	8	7	7	3	7	7	8	8	9	8	8	**8**
5	3	8	2	7	2	2	2	3	5	3	3	**3**
6	6	3	6	6	6	6	4	6	7	6	6	**6**
7	9	4	9	9	9	9	9	9	8	9	9	**9**
8	4	9	5	2	5	4	3	5	2	5	5	**5**
9	7	2	8	8	8	8	7	7	6	7	7	**7**
10	10	6	10	10	10	10	10	10	10	10	10	**10**
CORR % (with CR)	***98.4***	***-26.9***	***96.0***	***62.1***	***92.5***	***92.5***	***70.3***	***99.5***	***86.7***	***99.5***	***99.5***	**100.0**

Table 5: Corresponding correlations of each feature with the resulting cumulative ranks. The insignificant features are marked (Red) in the table.

The features which were detected to be below the **80% correlation threshold** are the Spectral Entropy (Spec. Entropy), The Inverse Difference Moment (IDM) and the Short

Run emphasis (SRE). The algorithm has been tested over a set of 10 unique test targets and also a set of 50 targets which consisted of 5 samples each for 3 printers and 4 media. These targets were subjectively observed by several PQEs and as expected, were classified to have some or large amounts of mottle. This can corroborated by the fact that the correlations between the CR and these features are low and these features do not characterize mottle. Thus, these features may be ignored from being included in the Spatio-frequency Mottle Metric (SFMM).

The next step is to compute the mottle metric that we proposed in the beginning of this thesis. This novel metric characterizes each sample based on the amount of mottle.

2.7 Relative and Absolute Mottle Metric

2.7.1 Relative SFMM - for multiple targets

As seen from the previous section, 8 significant features characterizing mottle are selected by the algorithm based on regression analysis using correlation. These features have values between 0 and 1, as shown in Table 2(c). This method is utilized to obtain a scale and a metric for a dataset of multiple test targets, in this case 10 K (black) only flat printed using 3 printers and 4 media as shown in Table 2(c). Given the nature of the features and how they were computed, the mottle metric is termed as the Spatio-Frequency Mottle Metric or SFMM. For clarity, SFMM for multiple test targets is called ‘Relative SFMM’ whereas for a single test target, it is known as ‘Absolute SFMM’ (explained in the next section). To obtain the Relative metric, all feature values shown in Table 2(c) were simply summed along the rows to obtain a single number associated with each target which is the above defined ‘Relative SFMM’. Eq. 28 represents the expression for each target’s SFMM value. Further, these 10 SFMM values are rank

ordered to obtain the relative ranks for the purpose of comparison with the subjective rankings.

$$SFMM_{R(i)} = \sum_{k=1}^{8} F_k \tag{28}$$

where $SFMM_{R(i)}$ represents the value of the mottle metric on a relative scale (subscript R) for the i^{th} test target (i ranges from 1 to 10) and F_k represents the k^{th} feature (k^{th} column) in Table 3. The final SFMM values are presented in Chapter 4.

2.5.1 Absolute SFMM – for a single target

As mentioned before, the primary objective of this work was to devise a metric that provides a measure of the amount of mottle on an absolute scale in comparison to a relative scale, which depicts the comparison of a test target with other targets in the dataset. For example, two targets may be selected randomly from a large data set known to have mottle and a rank on a relative scale. When these targets are evaluated in an isolated manner, that is, independent of each other, the two mottle numbers associated with each test target are expected to correspond with the behavior shown by the relative metric, hence providing the quality experts with a fair approximation of how much mottle there is in each target instead of a relative measure. Such a metric is proposed here, that provides an acceptably accurate absolute measure of the amount of mottle in each target.

Since in this case, there is only a single test target (single feature vector), the method of normalization was replaced by a method of weighting, where each feature was weighted based on its exponential powers. A logarithm based technique is used here, such that each feature is scaled down to a value between 0 and 10.

Firstly, any exponent powers acquired by these features are eliminated and brought to a scale between 1 and 10. This is done by the following set of equations:

$$\mu_{Raw} = \sum_{i=1toN} f_i \Big/ N \tag{29}$$

$$W_{feature} = 10^{-(\vartheta\{\log_{10}(\mu_{raw})\})} \tag{30}$$

where $\vartheta(x) = round(x)$ is an operator that rounds off x to the nearest integer.

The computed weight values for each feature ($W_{feature}$) are shown in form of exponent powers in Table 4(a). Note that, the features used for computing the absolute metric are the ones selected after the regression analysis done using the CR values. In this case, 8 raw feature values (see Table 1(a)) were used to compute the absolute metric as shown below:

$$SFMM_{Abs} = \sum_{k=1}^{8} W_k F_k \tag{19}$$

For clarity and better understanding of this section, we have provided the absolute SFMM values for the 10 test targets in Table 6(b) below along with the raw feature values from Table 1(a).

Feature	Mean Weight
Ring Mottle	X
ASM	$1 - X*10^{-1}$
ENTR	X
SFDA	X
LRE	$10 - X*10^{-3}$
GLNU	X*10-3
RLN	$X*10^{-2}$
RP	X

(a)

Test Target	Media	Ring Mottle	ASM	ENTR	SFDA	LRE	GLNU	RLN	RP	Absolute SFMM
1	Canon Color Laser	0.07	1.80	1.16	0.00	7959.48	1463.85	59.67	0.02	6.18
2	Hammermill Fore	0.12	2.37	0.14	0.02	4660.98	2775.90	108.07	0.02	10.27
3	Hammermill Laser	0.19	1.67	1.04	0.01	2621.02	2818.75	119.98	0.03	13.49
4	Xerox Bus. 4200	0.58	1.39	1.87	0.10	696.87	4190.66	397.43	0.05	20.93
5	Canon Color Laser	0.13	1.86	0.56	0.01	2714.67	3250.15	115.24	0.03	13.22
6	Hammermill Laser	0.46	1.49	1.59	0.04	1173.33	3422.95	225.58	0.04	17.49
7	Xerox Bus. 4200	0.80	1.22	2.24	0.15	677.50	3933.94	406.38	0.05	21.44
8	Canon Color Laser	0.18	1.57	1.32	0.01	2226.79	2774.58	130.46	0.03	14.24
9	Hammermill Laser	0.54	1.26	2.19	0.11	894.24	3405.38	312.86	0.05	19.40
10	Xerox Bus. 4200	1.15	0.96	3.00	0.74	379.88	4330.83	737.99	0.07	27.19

(b)

Table 6: Absolute SFMM; (a) empirically observed weight equations. Note that ASM and LRE are reversed (explained before) prior to calculation of Absolute SFMM. (b) Raw feature values from Table 2(a) for 10 test targets and their Absolute SFMM values computed using (a).

Chapter 3: Case Study on Color Test Targets

3.1 Introduction

The evaluation of achromatic test targets on the basis of mottle is a widely researched topic and has encouraged the print vendors and researchers to tackle the problem of colored mottle. This case study concerns with non-uniformities that occur due to all 4 printer primaries (C, M, and Y) when combined as halftones or solid areas. The aim of this case study is to apply the proposed algorithm to colored test targets.

There has been a considerable amount of concern amongst the researchers in this field to develop a universal metric for evaluation of mottle in color prints. A more recently proposed color mottle evaluation metric [14, 15] is based on prior work done [13] for evaluation of mottle in single channel (e.g. *K-only*). The model proposed in [14] is based on an assumption of conditional independence of channel information. We follow a different approach which utilizes the Principal Component Analysis. A similar approach was used by Ugbeme *et al.* [37] for detection of Debris Centered Deletion (DCD) defects in color printed targets.

The proposed method was validated on five preliminary test targets with the design pattern shown in Figure 13 below. The design pattern consists of Red, Green and Blue flat printed areas with varying amount of mottle. As these areas are larger than usual *K-only* targets used previously (830x830 pixels) and also not square contiguous, we use a

Divide-and-Cumulate feature computation technique (explained later) to evaluate each spatial and frequency domain feature for each colored area.

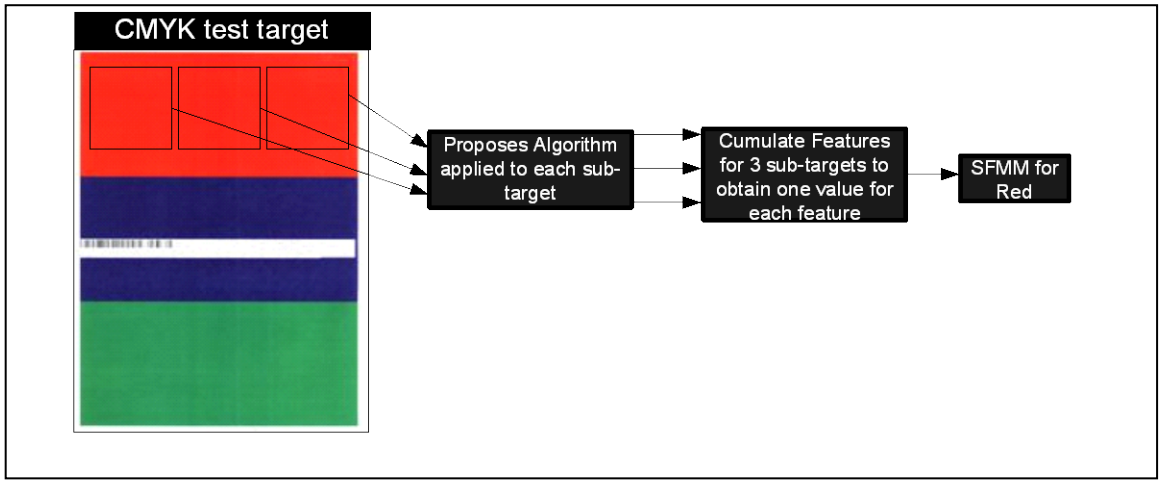

Figure 18: High level block diagram of the proposed algorithm for Color targets

3.2 Proposed PCA module for color targets

After the proposed algorithm was tested on about 70 K-only test targets, we performed the visual evaluations on these test targets. The idea behind evaluating the achromatic targets has been extended to evaluation of colored test targets. In an RGB image, it is hard to identify the channel which characterizes mottle. It is possible that there may be more multiple channels that are representative of the amount of mottle in the considered test target. The technique used here to extract information from all three channels (CMY or RGB) is known as Principal Component Analysis (PCA) [36]. A digitally scanned image is transformed into the CMY domain using simple linear transforms and this CMY image is sent through a PCA module to find the principal component (PC) corresponding to maximum energy or the maximum Eigen value. This component is used as the input to the SFMM algorithm. Note that, the PC obtained as a result is single channel and can be treated as a valid input to the SFMM algorithm.

To start with, we explain the process of principal component analysis [36] and its use and advantages in context to this work. The RGB scanned output, as mentioned previously, is converted to the CMYK intensity values using the following linear transformations:

$$C = G + B \tag{31}$$

$$M = R + B \tag{32}$$

$$Y = R + G \tag{33}$$

Principal Component Analysis (PCA) is a linear data reduction technique used to optimally project data, originally in a *d*-dimensional space onto a lower-dimensional space in a mean-squared error sense. The transformed axes are aligned with the directions of maximum variance of the data. Let ψ_1, ψ_2 and ψ_3 represent the three printer primaries C, M and Y. Then, $\Psi = [\psi_1 \quad \psi_2 \quad \psi_3]$, a 3 x N^2 matrix, is obtained by ordering each channel (C, M and Y) lexicographically where N is the x or y dimension of each image channel. The mean vector is computed next and is given by $m = [m_1 \quad m_2 \quad m_3]$ followed by the covariance matrix *V*, given by Eqns. (34) - (35).

$$\sigma_{\psi_k}^2 = E[(\psi_k - m_k)^2] = \frac{1}{N^2 - 1}\sum_{l=1}^{N^2}(\psi_k(l) - m_k)^2 \tag{34}$$

$$V = \begin{bmatrix} \sigma_{\psi_1}^2 & \sigma_{\psi_1\psi_2} & \sigma_{\psi_1\psi_3} \\ \sigma_{\psi_2\psi_1} & \sigma_{\psi_2}^2 & \sigma_{\psi_2\psi_3} \\ \sigma_{\psi_3\psi_1} & \sigma_{\psi_3\psi_2} & \sigma_{\psi_3}^2 \end{bmatrix} \tag{35}$$

where

$$\sigma_{\psi_k\psi_j} = E[(\psi_k - m_k)(\psi_j - m_j)^T] = \frac{1}{N^2 - 1}\sum_{l=1}^{N^2}(\psi_k(l) - m_k)(\psi_j(l) - m_j)$$

The covariance matrix, *C* is a real, symmetric and is expressed as:

$$V = E\Lambda E^T \tag{36}$$

where E is a 3 x 3 orthonormal matrix of eigenvectors corresponding to the ordered Eigen values $\lambda_1 \geq \lambda_2 \geq \lambda_3$ contained in the diagonal matrix $\Lambda = diag(\lambda_1, \lambda_2, \lambda_3)$. Finally, the principal components are computed as:

$$P = E^T \Psi = [P_1 \quad P_2 \quad P_3] \tag{37}$$

Hence, the variation of the original information is now distributed amongst the Eigen values where the first component P_1 corresponds to the component with largest variance. The first PC is henceforth selected as the input (high contrast gray-scale image) to the proposed SFMM algorithm explained in Chapter 2.

Note that, the above explained method works in an iterative way such that each color is divided into 3 sub-targets before the PCA. The proposed algorithm computes features for the three sub-targets and utilizes the average feature value for further steps. For simplicity, we name this technique as Divide-and-Cumulate. Note that, this methodology reduced the computational burden as the given test target patterns were large and rectangular in shape (as seen from Figure 18). After all features have been computed, the SFMM value is obtained using the proposed algorithm explained in Section 2. Results of this preliminary methodology are shown in Section 4 along with a brief discussion based on the nature of color mottle.

Subjective evaluations were not done for these sets of colored test targets; instead we provide a set of contrast enhanced images for the readers to perceptually evaluate mottle of the five color test targets used for this case study in Chapter 4.

Chapter 4: Experimental Results and Discussions

The proposed algorithm was tested with 70 printed outputs of 12 electronic originals obtained from 3 different printers and 4 different media. We divided these samples into 2 datasets. Set-1 consists of 10 test samples and Set-2 consists of 60 test samples which are primarily 12 test targets each printed 5 times. The correlation between the obtained SFMM rankings and subjective rankings obtained from 34 PQEs at Hewlett Packard company for 10 K-only targets (data set 1) ~ 94%.

The Visual Evaluation Procedure (VEP) is explained below followed by the results obtained from it. Next, the results of the algorithm are compared side by side with these subjective rankings and the visual metric. A brief discussion of results is provided at the end.

4.1 Visual Evaluation Procedure (VEP)

There have been many weighted sums based algorithms proposed to find one psychometric ranking derived from many human visual observers. A similar technique is used here to find the cumulative ranking which is described in [35].

Given 10 test targets, these are ranked in *r* different rankings according to *m* observers. First, a sum of rank values is computed using the following expression:

$$S_i = \sum_{k=1}^{n} f_{ik} R_k \tag{16}$$

where i represent the i^{th} image and varies from 1 to 10. The index k gives the rank and also varies from 1 to 10. The term f_{ik} represents the number of observers that give the i^{th} image a rank k. The term R_k is a vector in the reverse order to k and is given by $R_k = n - k + 1$. Finally, these values of S_i are arranged in descending order and the indices corresponding to this order are given as ranks to the images corresponding to i.

To corroborate the results of the algorithm, expert observers scaled these test targets visually under a standard set of conditions. The experiment was performed using pair-wise comparison (HP). A mottle value was given to each target based on its uniformity. A target that is flat and uniform is given a higher value than the target which is less uniform and contains more mottle. In this way, Print Quality Experts ranked these samples and the results obtained are shown below in Fig. 19 and Table 7.

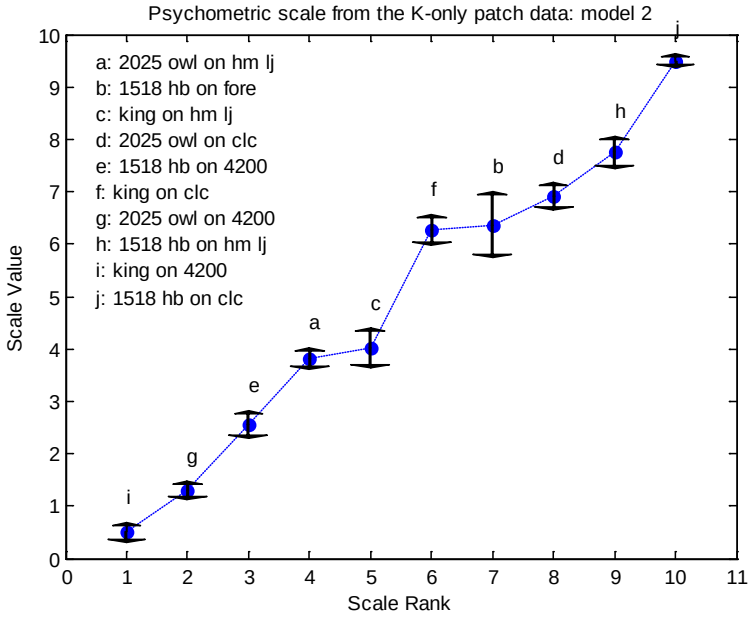

Figure 19: Visual scaling experiment results carried out at a HP facility by ~30 print quality observers. Scale Value / Scale Rank ~ 10 imply best print quality.

Printer	Media	VISUAL (M1)	VISUAL (M2)
1518	Canon Color Laser	**1**	**1**
1518	Hammermill Fore	**5**	**4**
1518	Hammermill Laser	**2**	**2**
1518	Xerox Bus. 4200	**8**	**8**
2025	Canon Color Laser	**3**	**3**
2025	Hammermill Laser	**7**	**7**
2025	Xerox Bus. 4200	**9**	**9**
King	Canon Color Laser	**4**	**5**
King	Hammermill Laser	**6**	**6**
King	Xerox Bus. 4200	**10**	**10**

Table 7: Tabulated summary of visual rankings along for two models.

In Table 7 there are numbers corresponding to the two models. The difference between the two is only between the number of subjects performing the experiment, that is, model 1 contains 18 observers and model 2 contains 30 observers. The difference between the rankings is not too large except in the case of two samples which can be explained by the increased number of observers.

The data obtained from visual scaling done at HP is then correlated with the results of the algorithm, that is, the SFMM rankings. The correlation observed was impressive at 96.5% except one target. The best sample has a value of 10, and the worst sample has a value of 0 on visual scale (See Table 7). In contrast, the SFMM provides the lowest value for the highest quality sample and the highest value for the worst quality sample.

4.2 Experimental Results

The experiments were performed on 70 test targets. All targets were from combinations of 3 printers – (1) 1518; (2) 2025; and (3) King and 4 printing media – (1) Canon laser color (2) Hammermill Fore; (3) Hammermill Fore and (4) Xerox business multipurpose 4200. The first data set, as mentioned before consists of 10 targets with the combinations shown in Figure 19(b). The second dataset consists of all ten possible combinations between the printers and media. Five test targets are produced for each combination, resulting in a total of 50 test targets.

The SFMM results were compared against those obtained from the VEP to analyze its overall performance. We compared the SFMM against the visual rankings obtained previously, on the basis of ranking-correlations.

4.2.1 Data Set 1 – 10 test targets

It is important to understand that the validity of the proposed algorithm can only be verified with testing on random test targets produced with a random amount of mottle. The targets in consideration in this section were carefully produced from 3 different printers using 4 different media. Note that, although three media (CLC, HML and XMB) have a sample each corresponding to the three printers (9 samples) but “Hammermill Fore” is only printed with printer 1 - 1518 making a total 10 targets.

This thesis presents a detailed analysis of with and without the Hammermill Fore sample. By removing the Hammermill Fore sample, the correlation increases significantly. The contrast enhanced test targets are shown in Figure 20(a) whereas their de-noised versions (input to the algorithm) are shown in Figure 20(b).

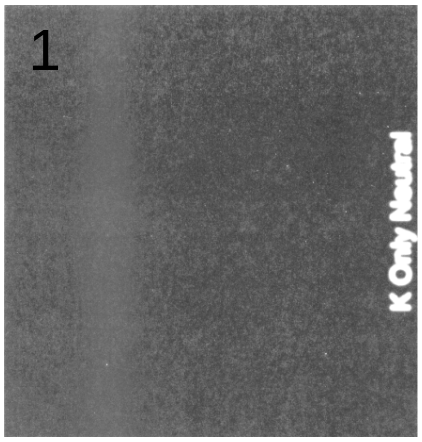

- Printer: 1518
- Media: Canon Laser

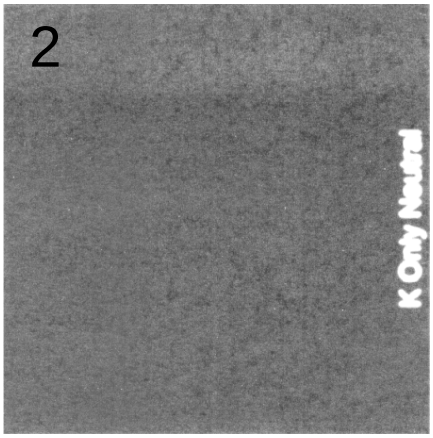

- Printer: 1518
- Media: HM FORE

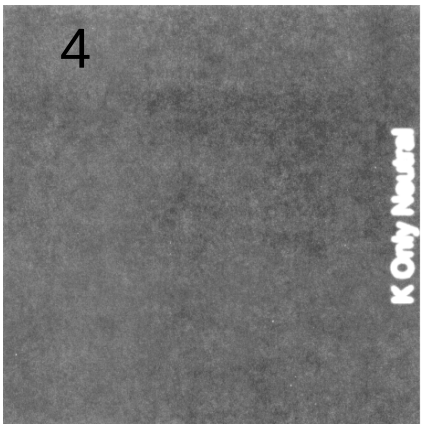

- Printer: 1518
- Media: HM Laser

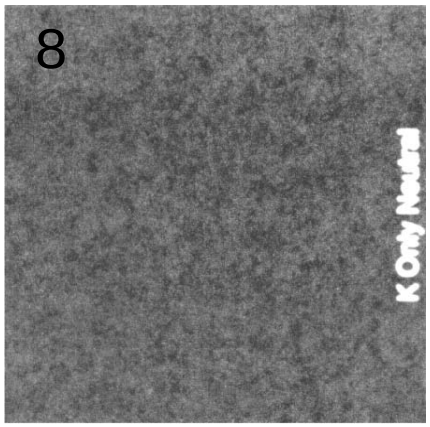

- Printer: 1518
- Media: XMB 4200

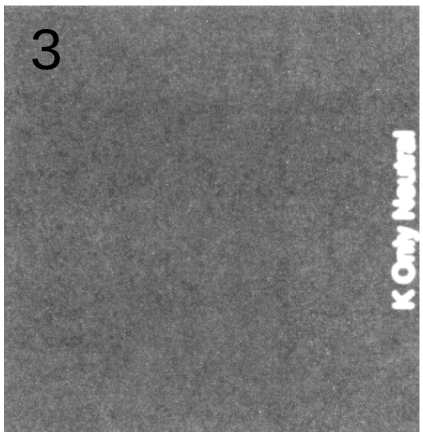

- Printer: 2025
- Media: Canon Laser

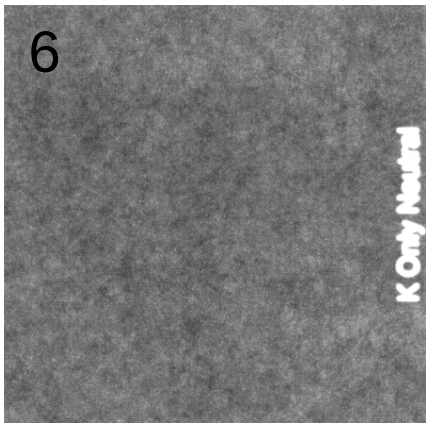

- Printer: 2025
- Media: HM Laser

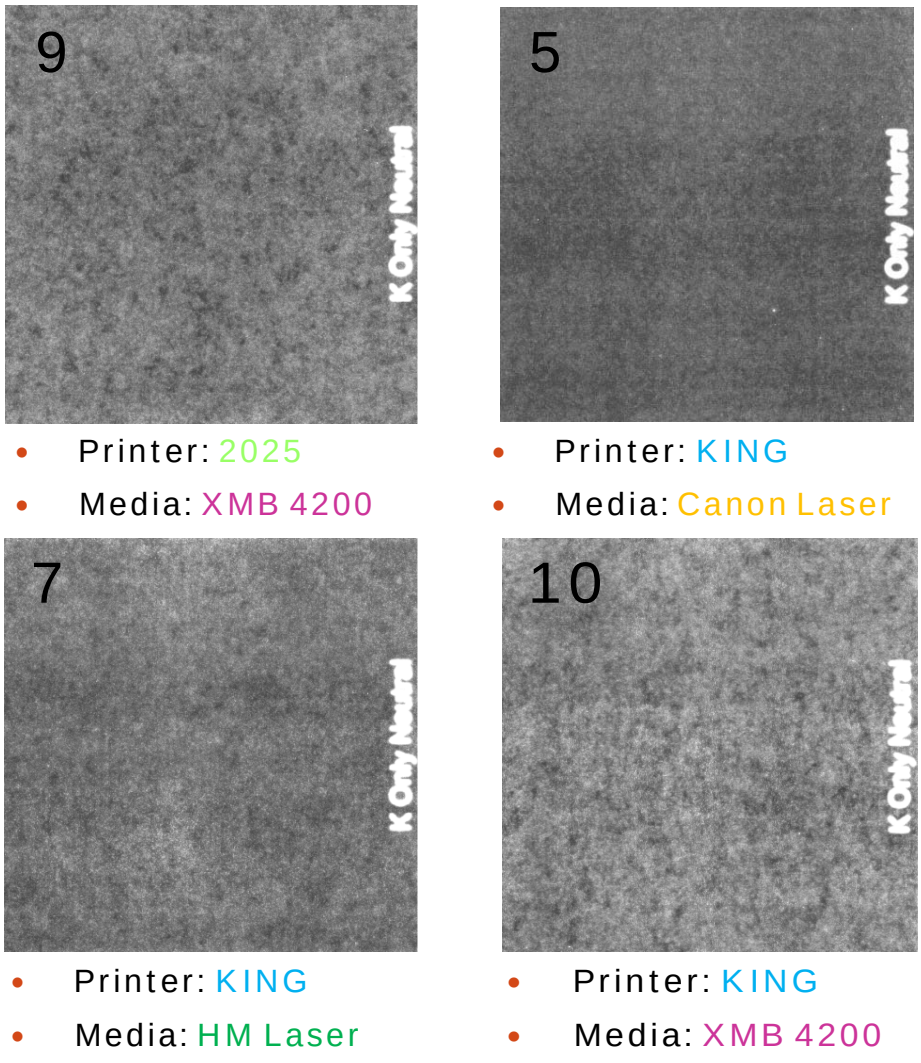

Figure 20: (a) 10 Test targets (contrast enhanced) used for validation of the algorithm.

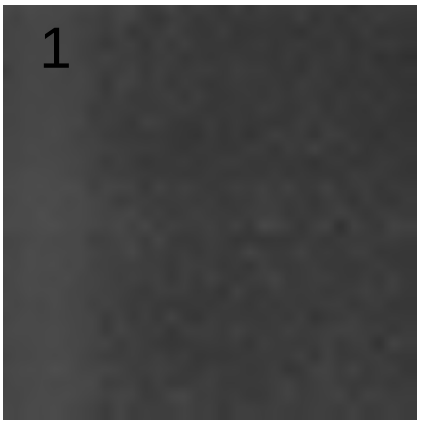

- Printer: 1518
- Media: Canon Laser

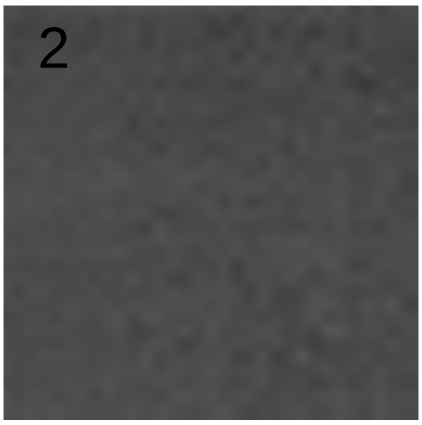

- Printer: 1518
- Media: HM FORE

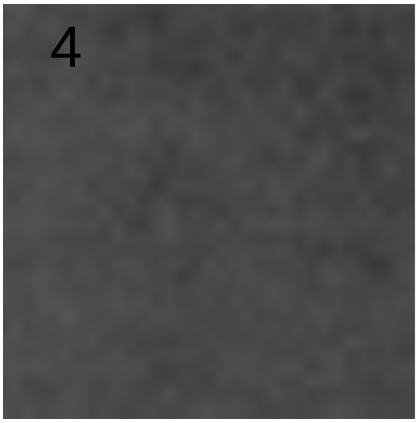

- Printer: 1518
- Media: HM Laser

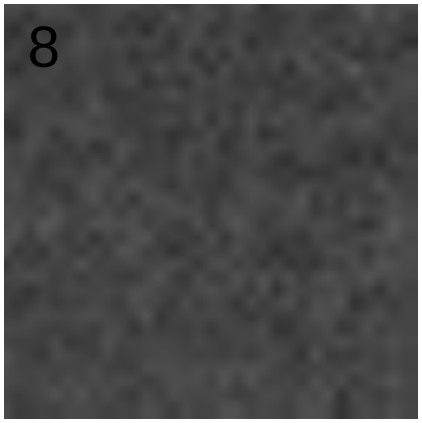

- Printer: 1518
- Media: XMB 4200

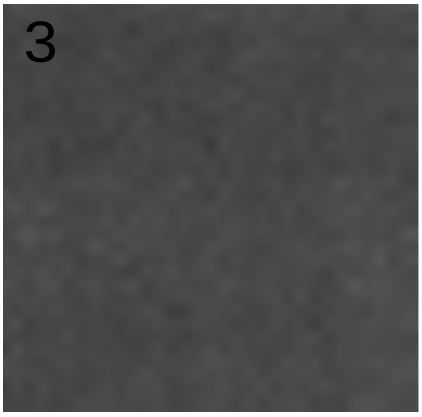

- Printer: 2025
- Media: Canon Laser

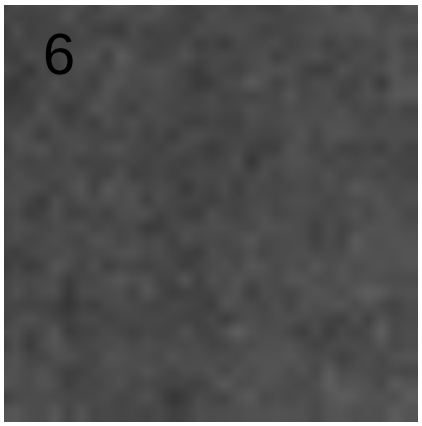

- Printer: 2025
- Media: HM Laser

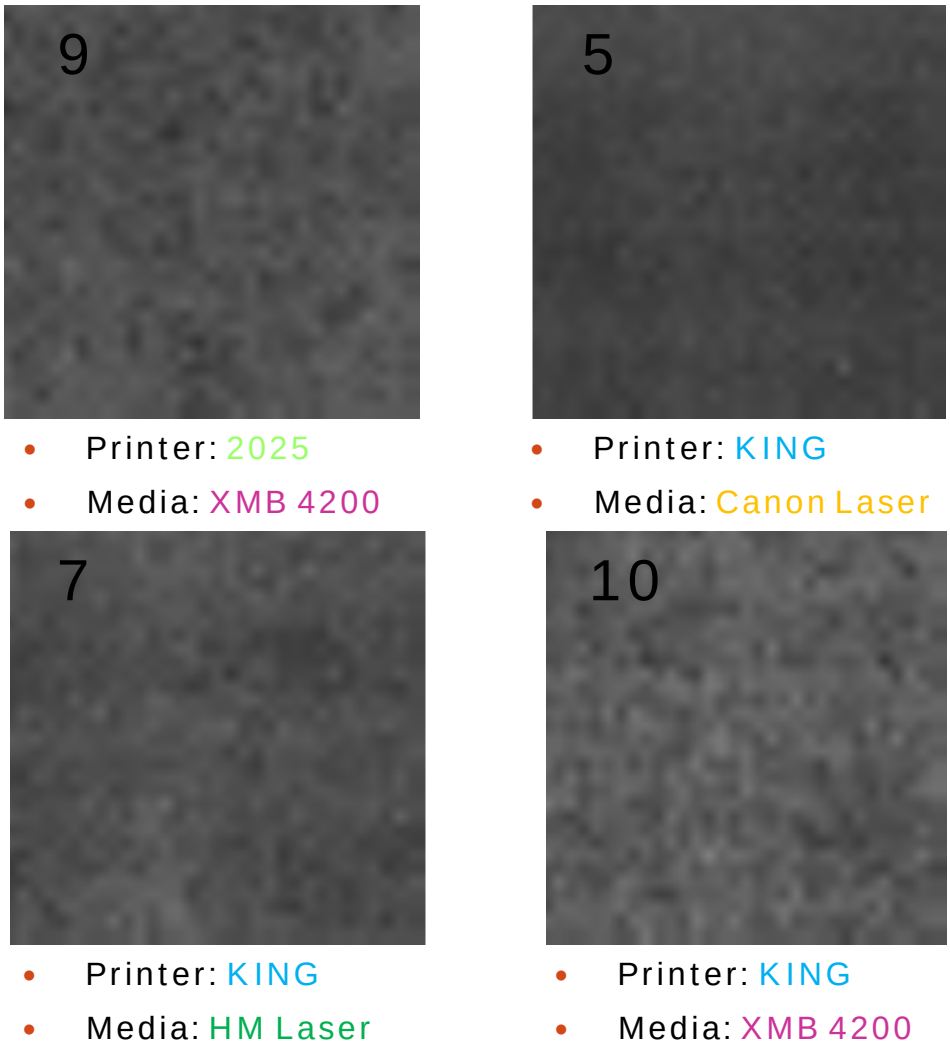

Figure 20: (b) De-noised versions of 10 Test targets (contrast enhanced).

4.2.2 Discussion

The graphical representation is shown in Figure 21 followed by a tabulated summary of SFMM, Visual Evaluation Procedure and their correlation in Table 8. It would be fair to say that the selected features for this data set are closely correlated. Together, these features are able to uniquely identify the test targets based on mottle (and sub-categories of mottle) as the spatial distribution (gray area non-uniformities) of each target is unique.

Different features computed in frequency and spatial domains are able to characterize these targets based on this different spatial frequency distribution.

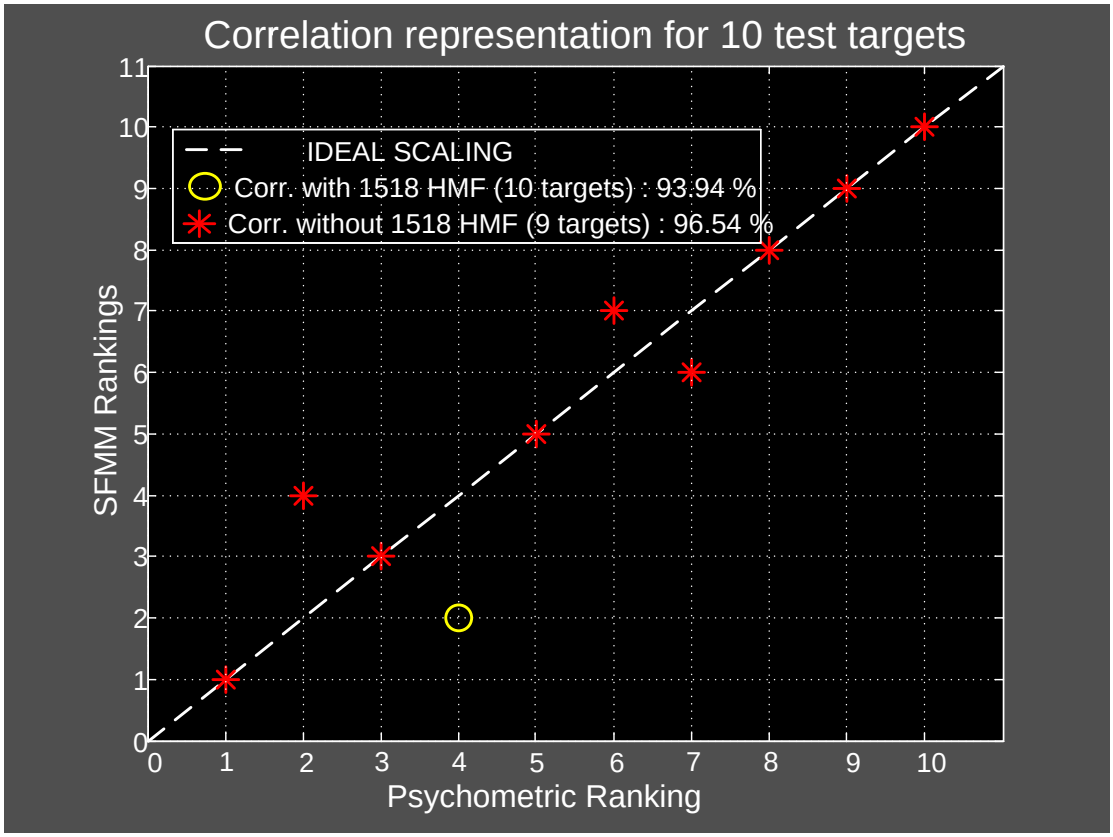

Figure 21: Correlation curve between SFMM (X axis) and Visual Rankings (Y axis)

In Fig. 21, a separated correlation distribution of test results is seen. An ambiguity where one of the samples - “1518 Hammer Mill Fore” was given a rank 5 on the uniformity scale by the observers and SFMM ranked it to be the best sample, lowers the correlation considerably from 96.5 % to 94%. We intend to look more carefully at this particular sample and find out why the disagreement exists.

In Table 8, a sorted list of data is given according to the scanning sequence of targets. In total 3 printers were used in generating the test targets – (1) “1518”; (2) “2025” and (3) “King”. Further, four different media were used to print about 20 test targets, 10 K Only

and 10 Process neutral. These media were – (1) Canon Color Laser (CLC); (2) Hammermill Fore (HMF); (3) Hammermill Laser (HML); (4) Xerox Business Multipurpose 4200 (Xx). The printer type and media type are mentioned for each test target in Table 5. Next, the selected features after the insignificant feature removal process are summarized for all targets along with the column with SFMM value. Note that the maximum SFMM value does not exceed the number of features for the worst sample (~8). This was done to maintain consistency and to identify the number of features finally included in evaluation of Absolute and Relative SFMM. The last two columns are replicated from Table 7 and consist of the VEP results.

Test Target	Printer	Media	Ring Mottle	ASM	ENTR	SFDA	LRE	GLNU	RLN	RP	Relative SFMM	RANK	Absolute SFMM	RANK	VISUAL (M2)
1	1	CLC	0.06	0.53	0.39	0.00	0.05	0.34	0.08	0.27	1.73	1	6.18	1	1
2	1	HMF	0.11	0.41	0.05	0.03	0.09	0.64	0.15	0.36	1.82	2	10.27	2	4
3	1	HML	0.17	0.59	0.34	0.01	0.11	0.65	0.16	0.41	2.45	4	13.49	4	2
4	1	XMB4200	0.51	0.70	0.62	0.13	0.34	0.97	0.54	0.75	4.56	8	20.93	8	8
5	2	CLC	0.11	0.51	0.19	0.01	0.09	0.75	0.16	0.41	2.22	3	13.22	3	3
6	2	HML	0.40	0.67	0.53	0.06	0.28	0.79	0.31	0.58	3.61	6	17.49	6	7
7	2	XMB4200	0.70	0.79	0.75	0.21	0.59	0.91	0.55	0.76	5.24	9	21.44	9	9
8	3	CLC	0.15	0.63	0.44	0.02	0.15	0.64	0.18	0.44	2.65	5	14.24	5	5
9	3	HML	0.47	0.76	0.73	0.15	0.33	0.79	0.42	0.67	4.32	7	19.40	7	6
10	3	XMB4200	1.00	1.00	1.00	1.00	1.00	1.00	1.00	1.00	8.00	10	27.19	10	10

Table 8: Spatio-Frequency Mottle Metric summary table for 10 test targets

Features from each test target were evaluated using the proposed algorithm. The 'Absolute SFMM' and 'Relative SFMM' values were computed and are shown in Table 8 above. Also shown is a regression curve depicting how well the subjective evaluations correlated with the objective results. It was seen that absolute and relative metrics correlated very well to each other as well as the subjective rankings. Another form of representation of results is given in Figure 22(a) where, the SFMM values and the VEP scale values are represented using a bar graph for a sample-by-sample based comparison. Figure 22(b) simply represents the SFMM ranks and the visual evaluation ranks

corresponding to the values shown in the previous table. Note that the SFMM bars are inverted using a linear transformation to plot them in accordance to the VEP scale (Highest value ~ Best Quality), hence a high value of SFMM represents a better rank (~ rank 1). In Fig. 21, a correlation distribution of results is seen. The observed correlation between the 'Relative' and 'Absolute' SFMM equal to 100% and each of them were found to be correlated to the subjective evaluations by ~ 94%. To test the robustness of the algorithm, we further tested 50 test targets that were essentially reproductions of the above 10 parent test targets (5 child targets for each parent) in order to report the consistency of the algorithm. From the above graphs, one major disagreement was observed in terms of subjective evaluations and proposed algorithm's results between two test targets – P1 HMF and P1 HML. This change did not affect the results much, as it was observed that removing the P1-HMF target increased the correlation to ~ 96%, showing a change of 2% only.

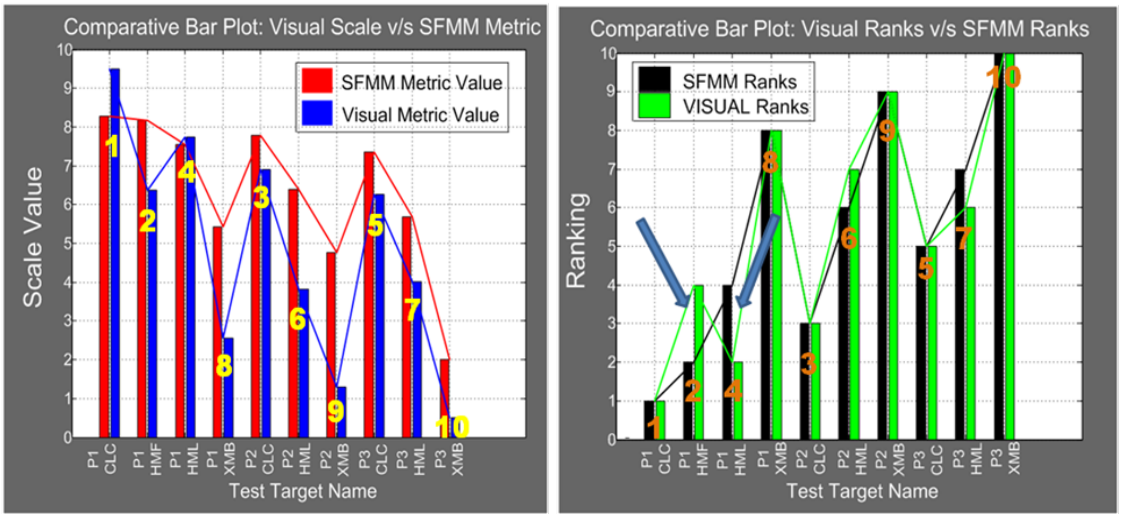

(a) (b)

Figure 22: Bar plot representation of SFMM values against the VEP results. (a) SFMM metric value versus the Visual Evaluation Scale; (b) SFMM Ranks versus the Visual ranks from (a).

It can be clearly seen from the results presented above and also is evident from Figure 12 that the most mottle was seen in targets printed using 'XEROX® Multipurpose Business 4200' or the XMB4200 which is a low grade copy paper, whereas the least mottle was observed in targets printed on 'Canon® Laser Color' which is a high grade photo printing paper. It has been a long known fact, that most of the mottle is introduced due to poor quality of the media, hence questioning the need for such an algorithm that characterizes printers only. It can easily be inferred that a high quality paper would introduce the least amount of mottle. A possible use of the proposed metric is for characterizing printers irrespective of the media or to compare behavior of mottle from several printers on the same media. This is the primary motivation for developing such an algorithm that rank orders the targets on an absolute as well as a relative scale. As seen from the results, the combination King-CLC is ranked amongst the worst half of the test targets with an 'Absolute SFMM' value more than twice the value for 1518-CLC, even though it is the best quality of media. This need for comparisons put across by print vendors serves the purpose for devising such algorithms.

4.2.3 Data Set 2 – 50 test targets

For the purpose of testing the robustness of the algorithm, a new dataset using the previously used three printers and four media (same as dataset 1), was generated by Hewlett Packard Company in form of fifty test targets where five targets corresponded to a single test target known as the parent target. A parent target is a unique combination of one printer and one media, hence giving us a total of 10 parent targets. Five child targets for each parent were generated one after the other in order to understand the consistency level of the algorithm in terms of repeatability and redundancy. The test targets were

divided into five batches – A, B, C, D, and E. Each batch consisted of ten unique child targets. To make the comparisons easier to interpret, five batches were evaluated using the algorithm repeatedly and the mean SFMM values for each parent target were computed by utilizing each batch's evaluation corresponding to that particular test target as shown in Table 10. Consequently, ten SFMM values for each unique parent are reported and finally rank ordered. Finally, error in the 'Relative SFMM' and corresponding ranks across the five batches are computed as the standard deviation for each parent target. As expected the proposed algorithm performed with minimal variation across the five batches.

Having obtained the 'Relative SFMM' statistics for this data set, there is still a need to determine how the 'Absolute SFMM' values are distributed across these fifty test targets. This application would be useful in case of two random test targets from different printers and the same media are to be compared. Another, useful application is when the effects of printing environment on the same combination of printer and media are to be recorded and corrected for. An absolute measure of the targets generated under different printing conditions would yield a better understanding of behavior of mottle for that combination of printer and media.

Table 9 shows these feature values for the 50 test targets. This feature matrix is divided into 10 groups along the rows signifying the uniqueness in respect to the printer name and media associated with it.

Test Target	Printer_Media_Run	Ring Mottle	ASM	Entropy	SFDA	LRE	GLNU	RLNU	RP
1	HB_CLC_A	0.108575	0.57444	0.45914	0.00705	0.02977	0.39866	0.32937	0.3911
2	HB_CLC_B	0.118072	0.56919	0.49492	0.01127	0.02894	0.3772	0.27664	0.37236
3	HB_CLC_C	0.1129	0.5074	0.53021	0.00576	0.02978	0.43373	0.32655	0.42618
4	HB_CLC_D	0.108845	0.50225	0.61775	0.00742	0.02967	0.37885	0.28293	0.37087
5	HB_CLC_E	0.102709	0.61738	0.4189	0.00584	0.03093	0.43874	0.32237	0.43122
6	HB_HMF_A	0.278536	0.49591	0.60779	0.06224	0.03519	0.42255	0.33279	0.44718
7	HB_HMF_B	0.270494	0.52825	0.48243	0.0708	0.06298	0.5572	0.41822	0.56038
8	HB_HMF_C	0.290613	0.50602	0.50937	0.10918	0.04372	0.47063	0.33738	0.47819
9	HB_HMF_D	0.293978	0.50483	0.54746	0.10806	0.04155	0.42833	0.30204	0.44298
10	HB_HMF_E	0.258674	0.59318	0.4132	0.07761	0.04252	0.475	0.36086	0.49532
11	HB_HML_A	0.19279	0.71966	0.23701	0.04777	0.06169	0.54296	0.39289	0.53951
12	HB_HML_B	0.17258	0.73226	0.1932	0.03309	0.0595	0.52164	0.36945	0.51619
13	HB_HML_C	0.180321	0.79749	0.01407	0.02156	0.12483	0.70407	0.51953	0.6949
14	HB_HML_D	0.197603	0.80264	-0.02281	0.01824	0.13627	0.72707	0.57135	0.71855
15	HB_HML_E	0.208927	0.837	-0.14377	0.04674	0.14451	0.78128	0.61186	0.77198
16	HB_Xx_A	0.493635	0.66043	0.31703	0.23446	0.08248	0.54739	0.46147	0.6069
17	HB_Xx_B	0.530491	0.61855	0.26196	0.25607	0.09032	0.48161	0.4746	0.61123
18	HB_Xx_C	0.529887	0.66325	0.24142	0.26798	0.10383	0.57752	0.53531	0.65723
19	HB_Xx_D	0.502172	0.55159	0.41141	0.189	0.07539	0.47837	0.3749	0.54817
20	HB_Xx_E	0.518846	0.55167	0.37091	0.24017	0.07179	0.4451	0.40486	0.5503
21	Owl_CLC_A	0.198473	0.6056	0.40593	0.05696	0.03281	0.44045	0.3397	0.45287
22	Owl_CLC_B	0.214845	0.48872	0.71982	0.0454	0.02689	0.30305	0.23553	0.33488
23	Owl_CLC_C	0.128093	0.48799	0.9828	0.01212	0.02345	0.16232	0.71569	0.14751
24	Owl_CLC_D	0.130878	0.48605	1	0.0092	0.02402	0.18342	0.49745	0.16806
25	Owl_CLC_E	0.123932	0.48822	0.92725	0.01006	0.02407	0.21628	0.33142	0.20379
26	Owl_HMF_A	0.331133	0.85733	-0.19266	0.08704	0.81139	1	1	1
27	Owl_HMF_B	0.280917	0.99447	-0.20471	0.08838	0.64243	0.98576	0.92414	0.97661
28	Owl_HMF_C	0.269802	0.9238	-0.19237	0.06166	0.18793	0.8929	0.7955	0.88531
29	Owl_HMF_D	0.281088	0.82691	-0.12922	0.05581	0.21348	0.91872	0.84226	0.91116
30	Owl_HMF_E	0.280603	0.83305	-0.14533	0.06065	0.25163	0.92559	0.84487	0.9182
31	Owl_Xx_A	0.717784	0.80189	-0.14576	0.63248	0.26924	0.82514	0.86631	0.93229
32	Owl_Xx_B	0.846185	1	-0.26966	0.36638	1	0.90055	0.83226	0.95684
33	Owl_Xx_C	0.502171	0.92488	-0.23999	0.26854	0.35926	0.92499	0.87445	0.94682
34	Owl_Xx_D	0.506304	0.97997	-0.20147	0.11919	0.28028	0.90183	0.75881	0.90127
35	Owl_Xx_E	0.440517	0.83803	-0.18642	0.14212	0.31461	0.92304	0.8318	0.93196
36	King_CLC_A	0.165465	0.75709	0.18811	0.04572	0.02592	0.29786	0.18428	0.30167
37	King_CLC_B	0.138197	0.73179	0.24503	0.03636	0.03503	0.43496	0.30423	0.43355
38	King_CLC_C	0.17689	0.70386	0.29846	0.02378	0.04239	0.49914	0.44074	0.49221
39	King_CLC_D	0.151661	0.51952	0.51904	0.01731	0.0276	0.35117	0.2534	0.35136
40	King_CLC_E	0.159903	0.73914	0.16087	0.02035	0.06234	0.54994	0.40071	0.5452
41	King_HLJ_A	0.313851	0.82033	-0.2418	0.09059	0.15074	0.68867	0.62954	0.78265
42	King_HLJ_B	0.323866	0.83808	-0.17675	0.08286	0.17178	0.78329	0.6459	0.79738
43	King_HLJ_C	0.350982	0.88359	-0.16831	0.09341	0.16462	0.7942	0.64073	0.7882
44	King_HLJ_D	0.480227	0.83407	-0.16699	0.16324	0.17988	0.81557	0.64458	0.81993
45	King_HLJ_E	0.428288	0.87148	-0.22024	0.10765	0.1777	0.78372	0.62791	0.81773
46	King_Xx_A	0.801137	0.81803	-0.30829	0.36989	0.19622	0.68972	0.84759	0.91264
47	King_Xx_B	0.852735	0.78634	-0.1628	0.65849	0.25894	0.76339	0.9406	0.94805
48	King_Xx_C	0.712224	0.78906	-0.20147	0.6214	0.17432	0.64002	0.70852	0.82645
49	King_Xx_D	0.903141	0.77858	-0.09948	0.68849	0.1848	0.68532	0.79338	0.89371
50	King_Xx_E	1	0.81952	-0.3002	1	0.2961	0.77173	0.87619	0.95083

Table 9: Feature Value matrix for Data set-2 consisting of 60 test targets.

The minimum SFMM value error observed in a test target across the five batches was ~ 0.18 (2025-HML) and a maximum of ~0.96 (2025-XMB4200). The maximum deviation seen across the ranks for each test target across the five batches did not exceed

~1.2. These results indicate that the proposed algorithm is consistent when tested for attributes like repeatability and redundancy. If an experiment was to be designed with an aim to obtain ideal printer performance characteristics for several printers, the proposed algorithm could prove to be efficient and acceptably accurate in terms of characterizing printers and suitable media based on mottle.

TEST TARGET INFO			BATCH										RELATIVE SFMM	
Parent No.	Printer	Media	A	Rank	B	Rank	C	Rank	D	Rank	E	Rank	SFMM (Mean ± Std. dev)	Rank (Mean ± Std. dev)
1	1518	CLC	1.55	3	1.36	2	1.13	2	1.36	3	0.97	2	1.27 ± 0.23	2 ± 0.55
2	1518	HMF	2.17	5	2.53	6	1.67	5	1.96	5	1.32	3	1.93 ± 0.46	5 ± 1.1
3	1518	HML	2.50	6	2.13	5	1.95	6	2.78	7	1.99	6	2.27 ± 0.36	6 ± 0.71
4	1518	XMB4200	3.35	7	3.29	7	2.64	8	2.65	6	1.99	7	2.78 ± 0.56	7 ± 0.71
5	2025	CLC	1.26	1	1.34	1	0.56	1	1.21	1	0.77	1	1.03 ± 0.34	1 ± 0
6	2025	HML	1.46	2	1.71	3	1.37	3	1.77	4	1.44	5	1.55 ± 0.18	3 ± 1.14
7	2025	XMB4200	5.90	10	5.43	9	4.14	10	4.69	9	3.51	9	4.73 ± 0.96	9 ± 0.55
8	KING	CLC	2.00	4	1.76	4	1.41	4	1.33	2	1.37	4	1.57 ± 0.29	4 ± 0.89
9	KING	HML	3.64	8	3.50	8	2.52	7	3.72	8	2.35	8	3.14 ± 0.66	8 ± 0.45
10	KING	XMB4200	5.25	9	5.75	10	3.78	9	5.10	10	4.31	10	4.84 ± 0.79	10 ± 0.55

Table 10: Results for 50 targets data set divided in to five batches along with **'Relative SFMM'** and corresponding rank statistics for ten test targets.

TEST TARGET INFO			BATCH										ABSOLUTE SFMM	
Parent No.	Printer	Media	A	Rank	B	Rank	C	Rank	D	Rank	E	Rank	SFMM (Mean ± Std. dev)	Rank (Mean ± Std. dev)
1	1	CLC	9.36	3	8.96	2	9.74	2	8.84	3	10.14	2	9.41 ± 0.54	2 ± 0.55
2	1	HMF	9.95	4	11.52	5	10.67	4	10.10	4	10.83	4	10.61 ± 0.63	5 ± 0.45
3	1	HML	11.73	6	11.58	6	13.60	7	13.85	7	14.52	7	13.06 ± 1.32	7 ± 0.55
4	1	XMB4200	12.08	7	12.03	7	12.60	6	11.38	6	11.36	5	11.89 ± 0.52	6 ± 0.84
5	2	CLC	7.20	1	7.93	1	0.43	1	2.09	1	3.82	1	4.29 ± 3.23	1 ± 0
6	2	HML	8.67	2	10.21	3	9.89	3	10.32	5	10.53	3	9.92 ± 0.74	3 ± 1.1
7	2	XMB4200	15.27	10	15.85	10	15.87	10	15.52	10	15.68	10	15.64 ± 0.25	10 ± 0
8	3	CLC	10.32	5	10.62	4	11.10	5	8.67	2	11.93	6	10.53 ± 1.2	4 ± 1.52
9	3	HML	14.38	8	14.68	8	14.70	9	14.89	9	14.82	8	14.69 ± 0.2	8 ± 0.55
10	3	XMB4200	15.01	9	15.18	9	14.31	8	14.52	8	15.44	9	14.89 ± 0.47	9 ± 0.55

Table 11: Results for 50 targets data set divided into 5 batches along with **'Absolute SFM**M' and corresponding rank statistics for ten test targets.

Another possible application could involve comparing one printer's performance across several media. To illustrate these applications, the 'Absolute SFMM' values for the 50 targets were evaluated and variations across the 5 batches for each test target are

shown with the help of a bar plot presented in Fig. 23. The variations are observed to be minimal as these test targets were printer under similar environments.

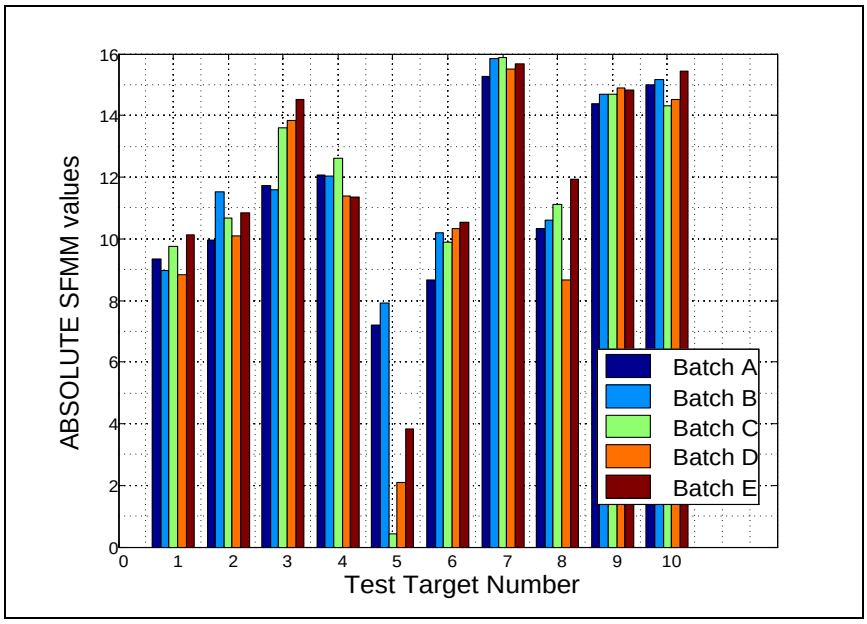

Figure 23: Comparison bar plot depicting variation level for each target across 5 batches.

The minimum 'Absolute SFMM' error observed in a test target across the 5 batches was ~ 0.2 (P3-HML) and a maximum of ~3.23 (P2-CLC). This unusually large variation was observed to be due to varying values of the features – LRE (Long Run Emphasis) and ENTR (Spatial Entropy). The cause of variations in these particular features in not known and currently being studied. There was no variation observed in the ranks across the 5 batches of P2-CLC, hence other causes for this large variation were not explored in detail. Maximum deviation seen across the ranks for each test target did not exceed ~1.6. Interestingly, it was observed that ranks for the ten test targets derived from the mean 'Absolute SFMM' did not vary much from those derived from the 'Relative SFMM' results. The results presented above are evidence of our proposed algorithm being

independent of a relative scale, hence providing a complete tool for evaluation of print mottle for any data set.

Prior to summarizing results for the color test targets, an important observation to be explained is the difference in results for dataset 1 (10 targets) and dataset 2 (50 targets) even though they are produced for similar combinations of printer and media. This proves that the phenomenon of print mottle is non-causal, that is, it is not necessary that the amount of mottle introduced by the same printer on the same media may remain constant under different conditions, such as time of printing, humidity and temperature. It also depends on the grade of toner used. Our research was focused on developing a model to help print vendors identify mottle and characterize targets after they have been printed. The above mentioned variations need to be accounted for, as an extension to this work but not in this thesis.

This concludes the results presented in for K-only samples. It is important to note that the test targets used here were printed using K color only and no halftones. It is also imperative to know that the proposed algorithm may perform differently for halftones and the spatial analysis may have to be adjusted accordingly.

4.2.4 Results for Color Test Targets (Chapter 4)

The proposed method for color targets was validated using 5 preliminary test targets with the design pattern shown in Fig. 13, presented earlier. The design pattern consists of red, green and blue flat printed areas with varying amount of mottle.

Shown in Figure 24 is one red test target along with each of the single channel images in RGB and CMY space. Also shown in this image is the first principal component selected that is essentially the grayscale input image for the proposed algorithm. All other

modules of the proposed algorithm remain unchanged and metric is calculated as shown above for the 5 color test targets for each color (R, G and B).

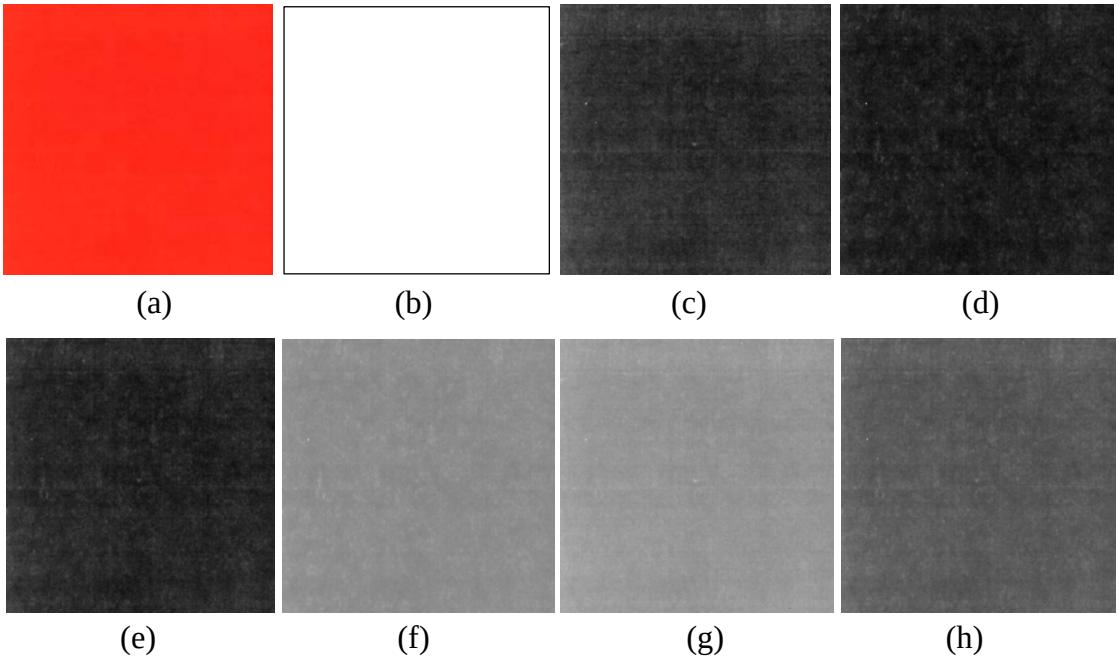

Figure 24: Example 'R' color test target with respective single channel images: (a) RGB, (b) R; (c) G; (d) B; (e) Cyan; (f) Magenta; (g) Yellow; (h) First Principal Component.

The image shown in Fig. 24(h) was used as the input to compute the 'Relative SFMM' values across the 5 colored test targets. The process was repeated for red, green and blue regions of the test target. Note that, the design of the test targets was such that red, green and blue regions share boundaries across the whole page. We utilized a color gradient based thresholding scheme to extract each color and store it as a separate image. Further, each color is evaluated one by one and the SFMM value is reported here. As the extracted colored sub-target is rectangular and larger in size in comparison to the conventional K-only design pattern used in the experiment before, it was further sub-divided into 3 equally sized targets (512x 512), as illustrated in Fig. 13 presented earlier, and their average SFMM value is reported as the final value for that color.

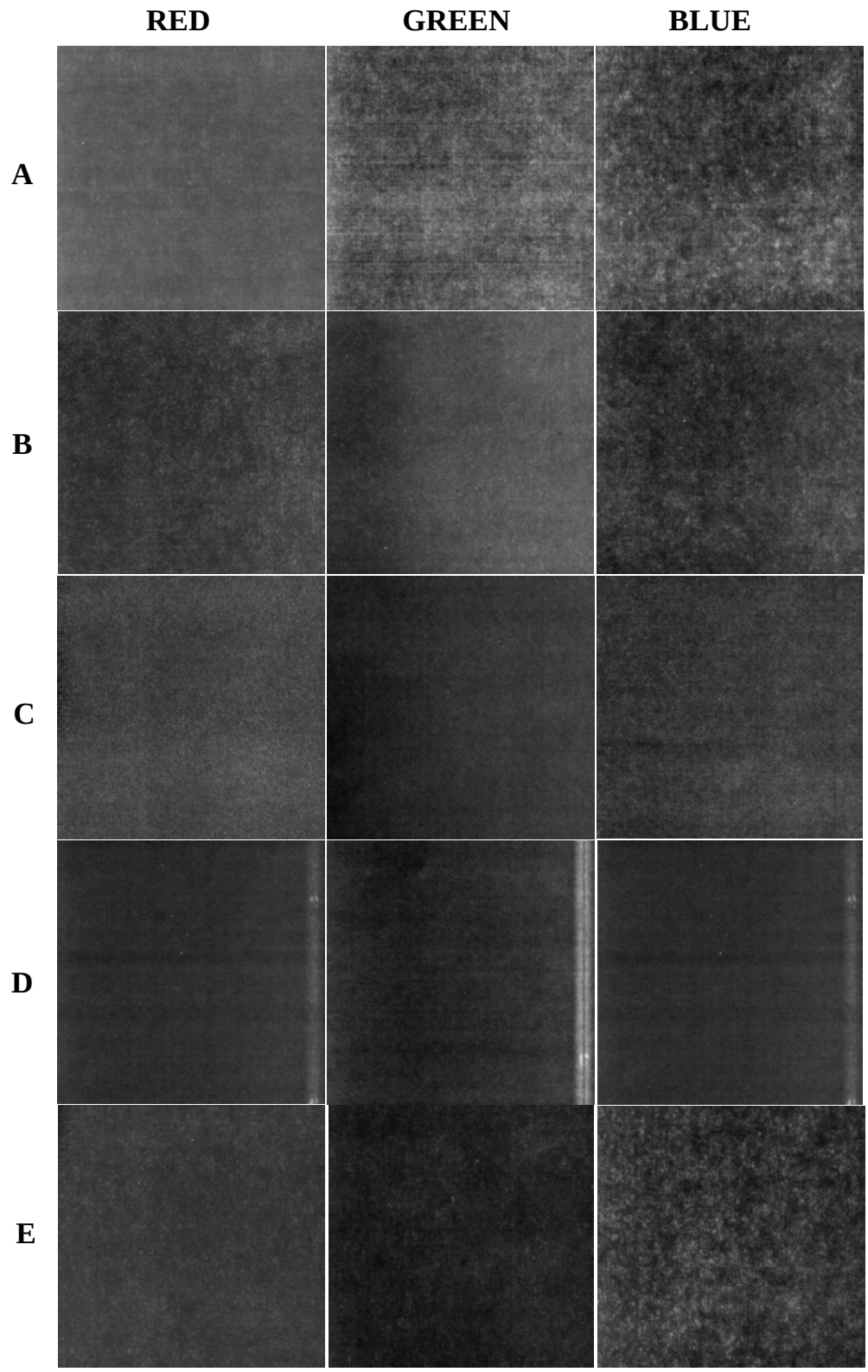

Figure 25: First Principal component of colored test targets indicated accordingly for 5 targets.

As there was no subjective experiment performed to evaluate these targets visually, there is no ground truth to compare the algorithm's results. For these reasons, the principal components extracted from the five test targets are presented in Fig. 16 to facilitate the reader comparing the results obtained from the algorithm with the reader's own results. This methodology needs to be validated on a greater number of test targets and compared with subjective evaluations obtained under laboratory controlled conditions.

Test Target	Color	SFMM	Rank	Probable Visual Rank
A	Red	8.98	5	5
	Blue	7.98	4	4
	Green	7.64	5	5
B	Red	6.88	4	4
	Blue	6.38	3	3
	Green	6.36	4	4
C	Red	1.92	1	2
	Blue	3.18	2	2
	Green	3.22	2	2
D	Red	2.16	2	1
	Blue	2.53	1	1
	Green	2.25	1	1
E	Red	3.85	3	3
	Blue	8.47	5	5
	Green	4.34	3	3

Table 12: Summary of Results for 5 color test targets (see Figure 25) with their probable visual ranks.

As mentioned earlier, it is left to the reader to evaluate these targets visually and compare them with the results of the algorithm. Principal components corresponding to each of the three printed colors from the five test targets are presented in Fig. 18. The amount of mottle in the target presented here can be perceived with ease, given that

observers are well-versed with the concept of print mottle and the perception properties related to it. These targets were accordingly evaluated with the help of a preliminary experiment performed by 5 trained observers. Readers may also be able to perform these experiments and approximately assign ranks to each target. These results are presented in Table 12 along with the SFMM values and corresponding ranks.

The visual ranks presented above may vary slightly from the reader's visual evaluations as the above rankings are representative of the mean rankings of a population of 5 observers. Note that this method requires modification using precise RGB-to-CMY look-up tables in order to quantify actual amount of mottle. The current technique utilizes a simple subtractive transformation as mentioned before in Chapter 3.

Considering the advantages of this new model over previous models available, the most important contribution is the introduction of a combinative analysis using spatial and frequency features with prior pre-processing using wavelets. To our knowledge, no attempt has been made to combine these features together and make a single model for evaluation of print mottle on a relative and, more importantly, an absolute scale using the same set of features.

4.3 Graphical User Interface

For the purpose of dissemination, a GUI was developed based on the proposed algorithm. It consists of two modes – "Single File Mode" and a "Multiple File Mode" which evaluate one file and multiple files (relative to each other) respectively. Snapshots of the two modes of the GUI are shown below in Figure 25.

(a)

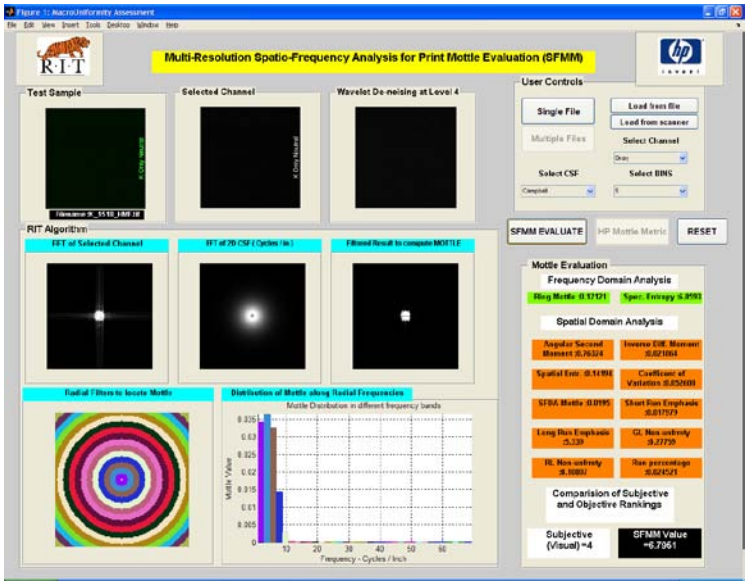

(b)

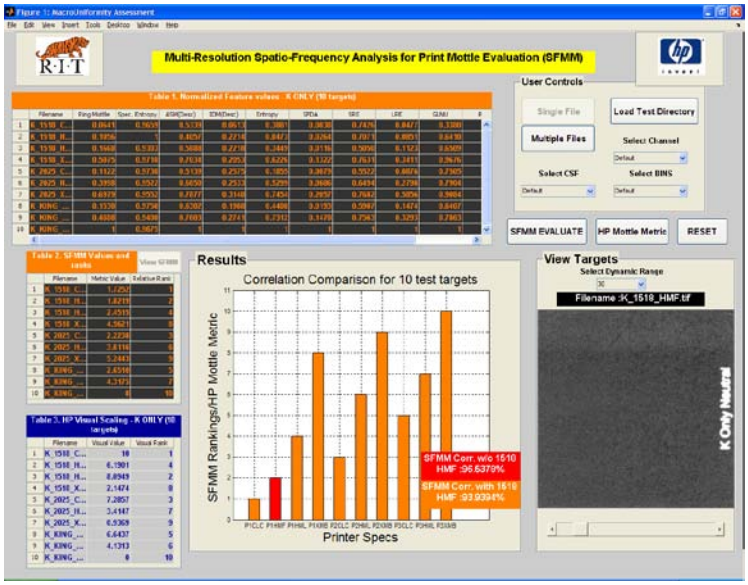

Figure 26: Graphical User Interface (GUI) in two modes: (a) Single File Mode; (b) Multiple Files Mode.

Chapter 5: Conclusions

This thesis proposes a methodology of evaluating only low frequency content using a novel combination of Spatial and Frequency domains with Wavelet domain preprocessing and also introduced a novel metric that provides a fairly accurate estimate of mottle in a given test target. The proposed metric - SFMM correlated well with the visual evaluation rankings ~ 96.5% for 9 test targets and 94% for 10 targets (including 1518 Hammermill Fore).

Two types of mottle metrics – 'Relative SFMM' and 'Absolute SFMM' were described and compared. The proposed algorithm was able to quantify mottle in a single target (Absolute SFMM) and was benchmarked successfully against the corresponding 'Relative SFMM' value with 100% accuracy. Both metrics were computed for 2 datasets of K-only flat printed test targets. Further, the SFMM rankings correlated to be at ~94% with the subjective evaluations performed by ~30 Print Quality Experts under laboratory conditions. Relative and Absolute SFMM values showed a similar behavior for the second data set and their respective ranks correlated with minimal variation. One important observation made from the results of the relative mottle metric and the features eliminated facilitated in selection of valid features for computation of the absolute metric. Features such as Spectral Entropy (E_{spec}), Short Run Emphasis (SRE) and Inverse Difference Moment (IDM) showed a low or even negative correlation for both datasets. Eventually, these features were not included in the computation of the 'Absolute SFMM' values. Given the performance of the proposed algorithm, we extended it to colored test targets by utilizing a PCA module for converting the image into a single channel image

as the input to the algorithm. Results were presented and correlated well with a preliminary subjective ranking obtained from 5 observers. Future work would include results from testing the algorithm on more color test targets given their subjective evaluations as well as modifying the proposed methodologies for evaluation of mottle in halftone prints.

Concerning the advantages of this new model over previous models available, the most important contribution is the introduction of a combinative analysis using spatial and frequency features with prior pre-processing using wavelets. After reviewing the literature, it is fair to say that no prior attempt has been made to combine these features together and make a single model for evaluation of print mottle. All our results, in fact, indicate that this rather straightforward method works well in a variety of printing conditions. The second important advantage of our approach is of the scanner being used. The scanned image, being acquired using 6 lamps and a customized routine adds to the algorithms robustness and eliminates any questions related to calibration and acquisition errors.

Addendum: Future Work

This work is proposed to be extended to another level of complexity. The next step would be to test the existing metric with more K-only targets for validation. It could then be developed into a complete robust tool to disseminate among the research community and the approach can also be extended for CMY solid prints and halftones.

Another scope lies in evaluation of print mottle in real life images. This is an area which still remains unexplored (See Fig. 26). Any such algorithm has, to our knowledge, not yet been published or developed. Currently, the proposed algorithm is compatible with only flat uniform images. But the existing algorithm can be integrated with a segmentation algorithm to extract the flat regions in the images and evaluate these regions for mottle. Real life images consisting of regions with varying levels of optical density and uniformity need to be handled and evaluated differently.

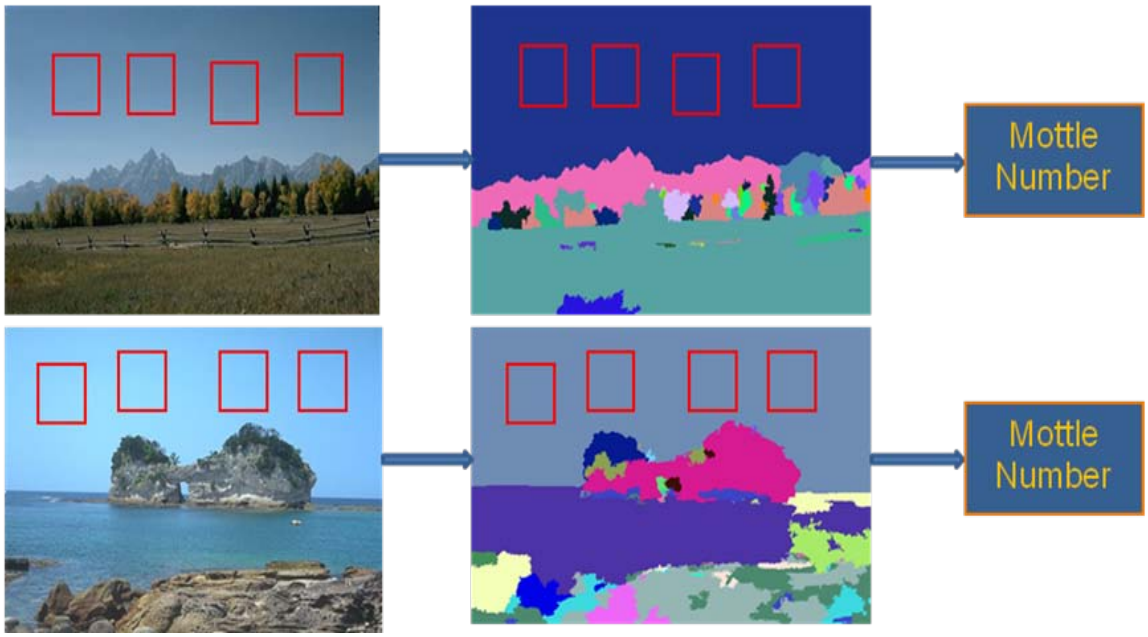

Figure 27: A proposed methodology to directly evaluate real life complex images, using the SFMM and the HP-RIT image segmentation algorithm.

References

1. D.R. Rasmussen, K.D. Donohue, Y.S. Ng, W.C. Kress, F. Gaykema, S. Zoltner, "ISO 19751 macro-uniformity," *Proc. SPIE Vol. 6059*,(2006), Image Quality and System Performance, Jan. 2006.
2. ISO/IEC DIS 13660 Draft International Standard, "Office Equipment – Measurement of image quality attributes for hardcopy output–Binary monochrome text and graphic images," *International Organization for Standardization*, ISO/IEC JTC1 SC28, 1996.
3. D.R. Rasmussen, K.D. Donohue, Y.S. Ng, W.C. Kress, F. Gaykema, and S. Zoltner, "ISO 19751 macro-uniformity," *Image Quality and System Performance III*, vol. 6059, 2006.
4. S.P. Farnand, E.N. Dalal and Y.S. Ng, "Recent progress in the development of ISO 19751," *Image Quality and System Performance III*, vol. 6059, San Jose, CA, 2006.
5. J.C. Briggs, D.J. Forrest, A.H. Klein, and M. Tse, "Living with ISO-13660: Pleasures and Perils," *Proc. of the IS&T's NIP15, Int. Conf. on Digital Printing Tech.*, Orlando, Florida, Oct. 1999.
6. M. Yuasa and P. Spencer, "NCITS-W1: Developing Standards for Copiers, Printers and Other Office Equipment," *Proceedings of IS&T's PICS*, pp. 270-273, Apr. 1999.
7. P. Spencer, "ISO 13660 New International Standard: Measurement of Image Quality Attributes for Hardcopy output–Binary monochrome text and graphic images," *IMI 2nd Annual Print and Image Quality Conference*, May 1997.
8. Applications of ISO-13660, A New International Standard for Objective Print Quality Evaluation.

9. D. Wolin, K. Johnson, and Y. Kipman, “The Importance of Objective Analysis in Image Quality Evaluation,” *IS&T's NIP 14: International Conference on Digital Printing Technologies*, Toronto, Canada, pp. 603-606, Oct. 1998.
10. P. Å. Johansson, “Print mottle evaluation by band-pass image analysis,” *Advances in Printing Science and Technology*, Vol. 22, Pentech Press, London, pp. 403, 1993.
11. C-M. Fahlcrantz, P. Å. Johansson and P. Åslund, “The influence of mean reflectance on perceived print mottle,” *Journal of Imaging Science & Technology,* Vol. 47, pp 54-59, 2002.
12. C-M. Fahlcrantz, “Evaluating Systematic Print Mottle,” *Journal of Graphics Technology,* Vol. 1, Issue 2, pp 19-28, 2003.
13. C-M. Fahlcrantz and P. Å. Johansson, “A comparison of different print mottle evaluation models,” *TAGA Proceedings,* San Antonio, 2004.
14. C-M. Fahlcrantz and J. Christoffersson, “Print mottle evaluation – An integrated approach,” *International conference on Printing Technology,* St. Petersburg, Russia, 2006.
15. C-M. Fahlcrantz and K. Sokolowski, “Evaluating color print mottle”, *33rd IARIGAI Research Conference,* Leipzig, Germany, 2006.
16. A.H. Eid, B.E. Cooper and E.E. Ripptoe, “Characterization of mottle and low frequency print defects,” *Proceedings of the SPIE,* Vol. 6808, pp. 680809-680809-12, 2008.
17. K. Donohue, C. Cui, and M.V. Venkatesh, “Wavelet analysis of print defects,” *Proc. of IS&T’s 2002 PICS Conference,* pp. 42-47, Portland, OR, 2002.

18. R. Dumas, S. Reele, and Y.Kipman, “Image Quality testing on the Production Line,” *Proceedings of IS&T’s PICS,* pp. 114-116, Mar. 2000.
19. P. Engeldrum, “Image Quality Modeling: Where Are We?,” *IS&T's PICS Conference,* pp. 251-255, Savannah (Georgia), Apr. 1999.
20. M. Tse, D. Forrest, and J.C. Briggs, “Automated Print Quality Analysis for Digital Printing Technologies,” *Pan-Pacific Imaging Conference/Japan Hardcopy*, pp. 15-17, Tokyo, Japan, Jul. 1998.
21. J.L. Crawford, C.D. Elzinga, and R. Yudico, “Print quality measurements for high-speed electro photographic printers,” *IBM J. Res. Dev.*, vol. 28, pp. 276-284, May 1984.
22. J. Raymond Edinger, Jr., “The Image Analyzer – A Tool for the Evaluation of Electrophotographic Text Quality,” *Journal of Imaging Science*, vol. 31, no. 4, July/August, 1987.
23. M. Tse, “Application of Automated Print Quality Analysis to Thermal Printing,” *IMI 9th Annual Thermal Printing Conference*, 1998.
24. B. Streckel, B. Steuernagel, E. Falkenhagen, and E. Jung, “Objective Print Quality Measurements Using a Scanner and a Digital Camera,” *International Conference on Digital Production Printing and Industrial Applications*, Barcelona, Spain, pp. 145-147, 2003.
25. P.J. Mangin and M. Dube, “Fundamental questions on print quality”, *Proc. of IS&T’s Electronic Imaging*, Vol. 6059, pp 605901-605901-12, 2006.
26. S.H. Kim and J.P. Allebach, “Impact of HVS Models on Model-based Halftoning”, *IEEE Transactions on Image Processing*, Vol. 11, Issue 3, pp. 258-269, 2002.

27. F.W. Campbell, R.H.S. Carpenter, and J.Z. Levinson, “Visibility of aperiodic patterns compared with that of sinusoidal gratings”, *J. Physiology,* vol. 204, pp. 283-298, 1969.
28. J.L. Mannos and D.J. Sakrison, “The effects of a visual fidelity criterion on the encoding of images.” *IEE Transactions on Information Theory,* vol. IT-20, July 1974.
29. R. Näsänen, “Visibility of halftone dot textures”, *IEEE Trans. Syst., Man, Cybern.,* vol. 14, no. 6, pp. 920-924, 1984.
30. S. Daly, “Subroutine for the generation of a Two dimensional Human Visual Contrast Sensitivity Function,” *Eastman Kodak, Tech. Rep. 233203y,* 1987.
31. P.J. Barten, “Physical model for the contrast sensitivity of the human eye,” in *Proc. IS&T/SPIE Int. Symp. On Electronic Imaging Science and Technology,* vol. 1666, San Jose, CA, Feb. 9-14, pp.57-72, 1992.
32. J.W. Cooley and J.W. Tukey, "An algorithm for the machine calculation of complex Fourier series," *Mathematical Computing vol.19: pp. 297–301,* 1965.
33. S. Theodoridis and K. Koutroumbas, “Pattern Recognition”, *Academic Press, Third Edition, pp 331-334,* 2006.
34. R. Rosenberger and D. Clark, “Stochastic Frequency Distribution Analysis as applied to inkjet print mottle measurement,” *Proc. of IS&T’s 17th Non-Impact Printing Conference,* pp-808-812, Fort Lauderdale, FL, 2001.
35. N. Abbadeni, D. Ziou and S. Wang, “Auto-covariance based perceptual textural features corresponding to human visual perception”, *Proc. of the 15th IAPR/IEEE Intl. Conference on Pattern Recognition,* pp 3913-3916, Barcelona, Spain, 2000.

36. J. E. Jackson, “A User’s Guide to Principal Components”, 1st ed., *John Wiley & Sons*, New York, 1991.

37. O. Ugbeme, E. Saber and W. Wu, and K. Chandu, "An Automated Algorithm for the Identification of Artifacts in Mottled and Noisy Images", *Journal of Electronic Imaging*, Vol. 16, No. 3, 2007.